

EarthArXiv Cover Sheet

Title

Large-scale Climate Modes Drive Low-frequency Regional Arctic Sea Ice Variability

Authors

Christopher Wyburn-Powell¹, Alexandra Jahn¹

Affiliations

¹Department of Atmospheric and Oceanic Sciences, and Institute of Arctic and Alpine Research, University of Colorado Boulder, Boulder, Colorado

Corresponding author

C Wyburn-Powell, chwy8767@colorado.edu

Peer-review statement

This manuscript is submitted to Journal of Climate and is **not** peer-reviewed. This preprint has been submitted to EarthArXiv.

1 **Large-scale Climate Modes Drive Low-Frequency Regional Arctic Sea Ice**
2 **Variability**

3 Christopher Wyburn-Powell^a, Alexandra Jahn^a

4 ^a *Department of Atmospheric and Oceanic Sciences, and Institute of Arctic and Alpine Research,*
5 *University of Colorado Boulder, Boulder, Colorado*

6 *Corresponding author: C Wyburn-Powell, chwy8767@colorado.edu*

7 ABSTRACT: Summer Arctic sea ice is declining rapidly but with superimposed variability on
8 multiple timescales that introduces large uncertainties into projections of future sea ice loss. To
9 better understand what drives at least part of this variability, we show how a simple linear model can
10 link dominant modes of climate variability to low-frequency regional Arctic sea ice concentration
11 (SIC) anomalies. Focusing on September, we find skillful projections from global climate models
12 (GCMs) from the Coupled Model Intercomparison Project Phase 6 (CMIP6) at lead times of 4-20
13 years, with up to 58% of the low-frequency variability explained by our linear model at a 5-year lead
14 time. The dominant driver of low-frequency SIC variability is the Interdecadal Pacific Oscillation
15 (IPO) which is positively correlated with SIC anomalies in all regions up to a lead time of 15
16 years, but with large uncertainty between GCMs and internal variability realization. The Niño 3.4
17 Index has good agreement between GCMs of being positively correlated with low-frequency SIC
18 anomalies for up to approximately 12 years. The Atlantic Multidecadal Oscillation is simulated as
19 being negatively correlated for up to approximately 10 years. No other climate modes investigated
20 were found to be of high importance in driving low-frequency Arctic SIC anomalies. Our results
21 suggest that, based on the 2022 phases of dominant climate variability modes, enhanced loss of
22 sea ice area across the Arctic is likely during the next decade.

23 SIGNIFICANCE STATEMENT: The purpose of this study is to better understand the drivers of
24 low-frequency variability of Arctic sea ice. Teasing out the complicated relationships within the
25 climate system takes a large number of examples. Here we use 42 of the latest generation of global
26 climate models to construct a simple linear model based on dominant named climate features to
27 predict regional low-frequency sea ice anomalies at a lead time of 2-20 years. In 2022, these
28 modes of variability happen to be in the phases most conducive to low Arctic sea ice concentration
29 anomalies. Given the context of the longer-term trend of sea ice loss due to global warming, our
30 results suggest accelerated Arctic sea ice loss in the next decade.

31 **1. Introduction**

32 Over the past four decades, summer Arctic sea ice has rapidly declined and is projected to
33 continue to decline in the future (Wang and Overland 2012; Notz and Stroeve 2016; Sigmond
34 et al. 2018). However, large variability on multiple timescales is superimposed on this declining
35 trend, which can lead to 10-20 year periods of accelerated sea ice loss but also to a period of
36 over a decade of no sea ice loss (Kay et al. 2011; Swart et al. 2015). Hence, it is not unexpected
37 that no new record low September sea ice area has occurred since 2012 (Francis and Wu 2020),
38 in particular as September internal variability is currently elevated due to the decrease in the
39 mean sea ice state (Goosse et al. 2009; Jahn 2018; Mioduszewski et al. 2019). The shelf seas
40 have been the focus of the observed decline as well as of the impact of internal variability,
41 with lower average sea ice concentration and thinner ice making the area a hotspot of internal
42 variability over the past few decades (Lindsay and Zhang 2006; England et al. 2019; VanAchter
43 et al. 2020; Årthun et al. 2021). The shelf seas are also coincident with areas of interest for
44 shipping (Eguíluz et al. 2016; Melia et al. 2017), natural resource exploration (Petrick et al.
45 2017), and ecological changes (Kovacs et al. 2011). However, the current characteristics of
46 variability are likely transitory as the shelf seas in the next few decades will become more
47 reliably ice-free throughout the summer (Barnhart et al. 2016; Crawford et al. 2021), ending
48 the dominant role of internal variability in projection uncertainty for this region (Bonan et al. 2021).

49

50 The internal variability of Arctic sea ice acts on multiple timescales and has therefore been
51 challenging to cleanly separate from the forced response (Stroeve et al. 2007; Kay et al. 2011;
52 Swart et al. 2015; Dörr et al. 2023). High-frequency drivers such as atmospheric temperature and
53 wind anomalies are generally considered dominant over lower-frequency drivers (Ding et al. 2019;
54 Olonscheck et al. 2019), but separating the drivers is difficult due to large spatial and temporal
55 heterogeneity in variability (Onarheim et al. 2018). By defining low-frequency variability as
56 periods of at least 2 years, approximately one quarter of September pan-Arctic internal variability
57 can be accounted for by low-frequency variability in a sample of global climate models (GCMs)
58 (Wyburn-Powell et al. 2022). Although low-frequency variability is only a small component
59 of internal variability, it promises some longer term predictability, as the influence of initial
60 conditions and high-frequency drivers of variability decay rapidly beyond the current season
61 (Blanchard-Wrigglesworth et al. 2011; Bonan et al. 2019; Bushuk et al. 2019), and have been
62 shown to be useful to a maximum of two year lead time (Day et al. 2014; Yeager et al. 2015;
63 Bushuk and Giannakis 2017; Holland et al. 2019; Gregory et al. 2021; Wang et al. 2021).

64
65 There is some prospect of summer Arctic sea ice predictability at lead times greater than 2
66 years due to ocean heat transports (Zhang and Wallace 2015; Docquier et al. 2021) and climate
67 modes of variability (Guemas et al. 2016). However, results so far seem to be model dependent
68 (Tietsche et al. 2014; Blanchard-Wrigglesworth and Bushuk 2019), and our current length of
69 observations is likely too short to verify such relationships (Bonan and Blanchard-Wrigglesworth
70 2020). Despite these challenges, extra-tropical modes of sea level pressure variability have
71 been suggested to have an influence on the Arctic sea ice variability, but so far only with strong
72 evidence on high-frequency timescales (Ukita et al. 2007; Serreze et al. 2007; L'Heureux et al.
73 2008; Zhang et al. 2019; Liu et al. 2021). Tropical teleconnections have also been identified
74 as influencing Arctic sea ice loss, primarily associated with Pacific sea surface temperatures
75 (SSTs) (Hu et al. 2016; Li et al. 2018a; Screen and Deser 2019; Ding et al. 2019; Kim et al.
76 2020; Clancy et al. 2021; Jeong et al. 2022b; Simon et al. 2022), but also with Atlantic
77 variability (Day et al. 2012; Miles et al. 2014; Meehl et al. 2018; Li et al. 2018b). These
78 insights into low-frequency drivers of variability show promise, but skillful regional predictions

79 combining multiple modes of variability at low-frequency timescales has so far been elusive.

80
81 Assessing drivers of low-frequency variability in the climate system is difficult to do without
82 large quantities of consistent data, such as that available from single model initial-condition large
83 ensembles (Deser et al. 2020; Milinski et al. 2020). This requirement for assessing drivers of
84 low-frequency Arctic sea ice variability stems from a multitude of drivers likely interacting on
85 heterogeneous spatial and temporal scales to cause this variability (Zhang et al. 2020). This has,
86 so far, lead to a lack of consensus of many of the drivers at time periods in excess of 2 years,
87 especially as GCMs and observations have been shown to represent these relationships differently.
88 We therefore leverage all available GCMs from the Coupled Model Intercomparison Project
89 Phase 6 (CMIP6) archive to investigate model consensus of these low-frequency relationships.
90 Additionally, we do not prescribe the nature of any of these relationships such as linearity
91 and independence, and seek high spatial and temporal specificity. To enable interpretation
92 of these potentially complex relationships in the climate system we use machine learning
93 which has been used successfully before to explain patterns of surface climate variability (e.g.
94 Barnes et al. 2019; Labe and Barnes 2022). With this coherent approach to determine the
95 drivers of low-frequency Arctic sea ice variability on multiple timescales and locations, we
96 determine the modes of variability which are simulated to have the largest impact and use the
97 resulting model to make predictions of low frequency SIC variability over the next decade.

98 99 **2. Methods**

100 *a. Data sources*

101 In order to gather sufficient data of both climate modes of variability and associated sea ice
102 concentrations, we use 42 GCMs with historical CMIP6 forcing (O’neill et al. 2016). These
103 GCMs are those for which both monthly sea ice concentration is available and the full suite of
104 climate mode data has been processed using the Climate Variability Diagnostics Package (CVDP)
105 (Phillips et al. 2014). In total we use 609 realizations, from 42 GCMs and 23 modeling centers; a

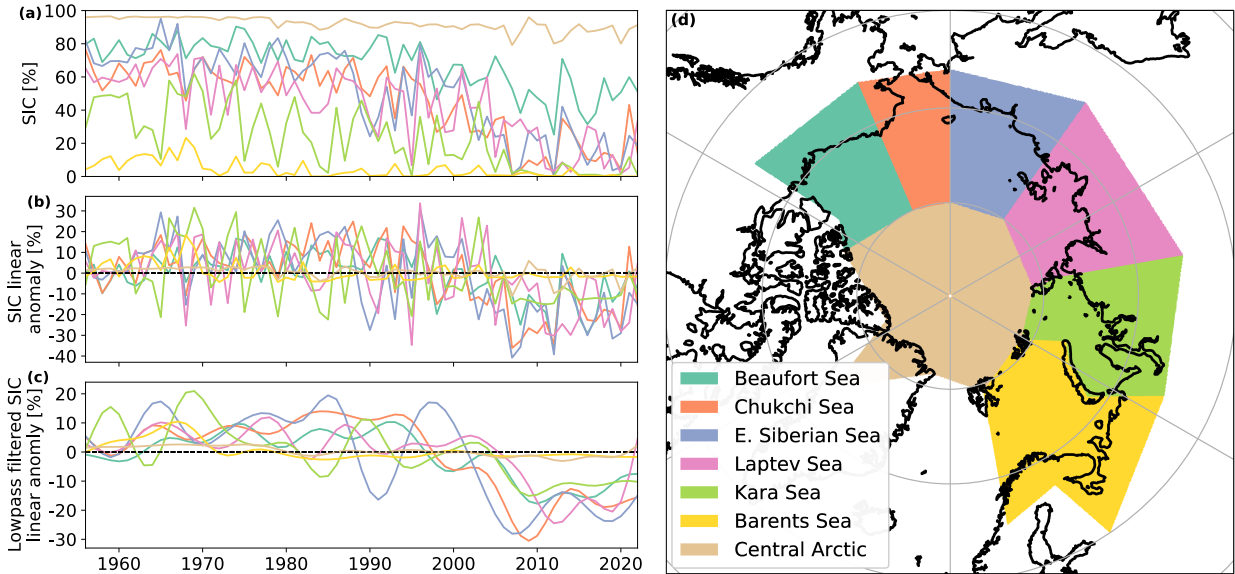
106 full list can be found in Table 1. The only other simulations which could provide a similarly large
107 quantity of data would be future scenarios or pre-industrial control simulations. However, as the
108 mean-state and variability of the Arctic sea ice (VanAchter et al. 2020; Årthun et al. 2021) and
109 some aspects of the rest of the climate system such as ENSO (Brown et al. 2020) or AMOC (Weijer
110 et al. 2020) differ from present conditions in both the pre-industrial and future climate states, this
111 approach would be less appropriate to analyze current variability. Within the historical period we
112 use the 74-year time period 1941-2014 for sea ice concentration (SIC), which we average over
113 regions of the Arctic as defined by the National Snow and Ice Data Center (NSIDC) Multisensor
114 Analyzed Sea Ice Extent - Northern Hemisphere (Fetterer et al. 2010) (see Figure 1d). These
115 seven regions cover the vast majority of the sea ice found during the summer, although we do
116 exclude the Canadian Arctic Archipelago due to complex coastal zones which are typically poorly
117 represented in GCMs (Long et al. 2021). We linearly detrend the average SIC for each region
118 (for the period 1920-2014) and then apply a 2-year lowpass filter to exclude the high-frequency
119 interannual variability and leave only the low-frequency anomalies (see Figure 1a-c). This low-
120 pass filtered regional sea ice concentration data becomes the predictands in our regression analysis.

121
122 We use nine variables from the CVDP to assess their influence on regional SIC anomalies in our
123 regression analysis. We obtain seasonal values for all variability modes except the Interdecadal
124 Pacific Oscillation (IPO) where we use a single annual value. The seasonal or annual modes are
125 linearly detrended and standardized (if not already in such a format) but no other data transforma-
126 tions are made. We use data from 1920-2014 to facilitate lagging the SIC data between 2 and 20
127 years from the CVDP data. When we present the linear effects of each mode of variability, the
128 modes which have seasonal values are summed to produce a combined effect. The eight variables
129 used from the CVDP and their abbreviations are listed below:

- 136 • AMO: Atlantic Multidecadal Oscillation
- 137 • NAO: North Atlantic Oscillation
- 138 • ATN: Atlantic Niño
- 139 • NINO34: Niño 3.4 Index

TABLE 1. Global climate model output used in this analysis

Modeling Center	GCM Name	Members	Citation
CSIRO-ARCCSS	ACCESS-CM2	5	Dix et al. 2019
CSIRO	ACCESS-ESM1.5	40	Ziehn et al. 2019
BCC	BCC-CSM2-MR	3	Wu et al. 2018
BCC	BCC-ESM1	3	Zhang et al. 2018
CAMS	CAMS-CSM1.0	3	Rong 2019
NCAR	CESM2-FV2	3	Danabasoglu 2019a
NCAR	CESM2-LENS	50	Danabasoglu 2019b
NCAR	CESM2-WACCM	3	Danabasoglu 2019d
NCAR	CESM2-WACCM-FV2	3	Danabasoglu 2019c
THU	CIESM	3	Huang 2019
CMCC	CMCC-CM2-SR5	11	Lovato and Peano 2020
CNRM-CERFACS	CNRM-CM6-1	21	Voltaire 2018
CNRM-CERFACS	CNRM-ESM2-1	6	Seferian 2018
CCCma	CanESM5	65	Swart et al. 2019b
CCCma	CanESM5-CanOE	3	Swart et al. 2019a
E3SM-Project	E3SM1.0	4	Bader et al. 2019
EC-Earth-Consortium	EC-Earth3	23	EC-Earth-Consortium 2019a
EC-Earth-Consortium	EC-Earth3-CC	10	EC-Earth-Consortium 2021
EC-Earth-Consortium	EC-Earth3-Veg	7	EC-Earth-Consortium 2019b
EC-Earth-Consortium	EC-Earth3-Veg-LR	3	EC-Earth-Consortium 2020
FIO-QLNM	FIO-ESM2.0	3	Song et al. 2019
NOAA-GFDL	GFDL-ESM4	3	Krasting et al. 2018
NASA-GISS	GISS-E2-1-G	46	NASA Goddard Institute for Space Studies 2018
NASA-GISS	GISS-E2-1-H	25	NASA Goddard Institute for Space Studies 2019b
NASA-GISS	GISS-E2-2-G	11	NASA Goddard Institute for Space Studies 2019a
NASA-GISS	GISS-E2-2-H	5	NASA Goddard Institute for Space Studies 2019c
MOHC	HadGEM3-GC31-LL	5	Ridley et al. 2019a
MOHC	HadGEM3-GC31-MM	4	Ridley et al. 2019b
INM	INM-CM5-0	10	Volodin et al. 2019
IPSL	IPSL-CM6A-LR	32	Boucher et al. 2018
MIROC	MIROC-ES2H	3	Watanabe et al. 2021
MIROC	MIROC-ES2L	31	Hajima et al. 2019
MIROC	MIROC6	50	Tatebe and Watanabe 2018
HAMMOZ-Consortium	MPI-ESM1.2-HAM	3	Neubauer et al. 2019
MPI-M	MPI-ESM1.2-HR	10	Schupfner et al. 2019
MPI-M	MPI-ESM1.2-LR	30	Wieners et al. 2019
MRI	MRI-ESM2.0	12	Yukimoto et al. 2019
NUIST	NESM3	5	Cao and Wang 2019
NCC	NorCPM1	30	Bethke et al. 2019
NCC	NorESM2-LM	3	Seland et al. 2019
NCC	NorESM2-MM	3	Bentsen et al. 2019
MOHC	UKESM1.0-LL	16	Tang et al. 2019



122 **FIG. 1. Observed September sea ice concentrations for the seven Arctic regions used in this analysis.** The
 123 observational HadISST1 sea ice concentration data shown for (a) the regional average, (b) the linearly detrended
 124 version of (a), and (c) a 2-year lowpass filter applied on (b). What is shown in (c) is the data used in the analysis
 125 presented here. The outline of the different regions considered are shown in (d) and defined as for the National
 126 Snow and Ice Data Center (NSIDC) Multisensor Analyzed Sea Ice Extent - Northern Hemisphere (MASIE-NH)
 127 dataset (Fetterer et al. 2010).

- 140 • PDO: Pacific Decadal Oscillation
- 141 • NPO: North Pacific Oscillation
- 142 • PNA: Pacific/North American Teleconnection
- 143 • IPO: Interdecadal Pacific Oscillation

144 In addition to these modes of variability, we also include the seasonal values
 145 of the global average surface temperature (TAS), as motivated in section d.

146
 147 Several additional modes of variability were also available from the CVDP but were not
 148 included in the final analysis. The modes investigated but not used are as follows: the Indian
 149 Ocean Dipole, the Atlantic Meridional Mode, the Southern Annular Mode, the North Pacific

150 Index. All of these modes of variability had no measurable effect on the regression model. Fur-
151 thermore, including the Northern Annular Mode lead to over-fitting with the highly related NAO.

152

153 Observational SIC is taken from the Hadley Centre Sea Ice and Sea Surface Temperature
154 data set (HadISST1) (Rayner et al. 2003) for the period 1956-2022. We use the HadISST1
155 SIC record before the beginning of the satellite era in 1978 to enable longer analyses in our
156 correlation analysis in section e. 1956 is the starting year of the SIC data we use as variability
157 is degraded substantially before 1956 due to interpolations for September-March (Rayner et al.
158 2003). However, when calculating a linear trend for detrending, we use SIC data for 1920-2014
159 in order to be consistent with the GCMs. The HadISSST1 data, similarly to the SIC in the
160 GCMs, is divided into regions, linearly detrended and interannual variability is removed with a
161 2-year lowpass filter. For observed climate variability data we also obtain these from the CVDP
162 where we use the HadISST1 dataset to calculate sea surface temperature-derived variables, the
163 NCEP-NCAR record for sea level pressures (Kalnay et al. 1996), and GISTEMP version 4 for
164 global surface temperatures (Lenssen et al. 2019). Similarly to the CVDP output variables for the
165 GCMs, we apply a linear detrending and standardization to the variables not already in this format.

166

167 *b. Machine Learning Methods*

168 The aim of using machine learning is to determine the relationship between the climate
169 variability modes and the lagged effects on regional Arctic SIC gain and loss. We provide the
170 CVDP variables as feature inputs to regress SIC anomalies 2 to 20 years later, for a given region
171 and month of SIC anomalies. To do this, many realizations are required to provide sufficient
172 training data; our one realization of reality from observations does not provide a long enough
173 time period in which to disentangle the relationships between climate variability modes and
174 regional SIC anomalies. We compute regressions both for an individual GCM large ensemble
175 (LE) which we require to have at least 20 members (12 large ensembles in total), and also two
176 CMIP6 multi-model large ensembles comprising of GCMs with at least 3 members (n=42) or 30
177 members (n=8), referred to as MMLE 3+ and MMLE 30+ respectively. For each LE we divide the

178 members into training, validation, and testing sets with 75%, 15%, 10% of members respectively,
179 similar to theoretical 'optimal' splits for 33 variables such as 72/13/15% from Joseph 2022. For
180 the MMLE 3+ we select all of the GCMs which provide at least 3 realizations, then we use the
181 first member for the training data set, the second member for the validation set, and leave the third
182 and any other members for testing. For the MMLE 30+ we pool the first 23 members from all 8
183 GCMs for training, we use the next 4 members for validation, and the final 3 or more members for
184 testing. As we use 74 years of data for each ensemble member the smallest LE uses 74 years with
185 21 ensemble members, yielding an effective 1554 years for training - far in excess of observations
186 and typically longer than pre-industrial control runs from any individual GCM. On the other
187 extreme, the MMLE 30+ maximizes the number of effective training years at 13,320, allowing us
188 to determine whether substantially increasing the training data provides any gain in predictive skill.

189
190 We make use of 8 climate modes of variability and TAS, where all except the IPO have four
191 seasonal values. Hence our total is 33 input feature variables in our regression analysis. Our
192 objective is to assess the effect of each of these variables as a function of time preceding the
193 target regional SIC anomalies for a given month. Therefore, we train our machine learning
194 models on a single region, month, and lag time. This granularity of regression analysis allows us
195 to determine the different links between climate modes and SIC anomalies across regions, SIC
196 anomaly months, and lag time, without prescribing assumptions regarding regional or temporal
197 evolution. The SIC anomalies are in % points, hence when comparing the influence of modes of
198 variability across regions, the % point change should be scaled by the variability of that region.
199 Our model has no knowledge of the initial anomaly of SIC, but as the memory for the summer
200 at lead times in excess of 1 year is considered negligible (Giese et al. 2021), this omission is
201 considered unimportant at the timescales we consider. Furthermore, this would add additional
202 complexity to our model by adding degrees of freedom which would require more data to constrain.

203
204 For the 12 LE and 2 MMLE data sets, we devise four experiments with different machine learning
205 model configurations to investigate the effect of nonlinearities and interdependence between climate
206 variability modes in skillful prediction of regional SIC anomalies. All of the four machine learning
207 models use a fully-connected neural network with the same L1 loss function to encourage sparseness

208 and an Adam optimizer for suitability to the four diverse experiments. There is no bias used for
209 models 1 and 2 as this allows direct analysis of the linear effect of the input variables and is
210 permissible as we are using standardized values for our features. With these four machine learning
211 models, as detailed below, we can separate the effect of linear/nonlinear activation functions from
212 the effect of additional neural network layers which allows one climate variable to interact with
213 another:

- 214 • Model 1 - Model layers: 33-1 with linear activation functions and no bias.
- 215 • Model 2 - Model layers: 33-1 with nonlinear (ReLU) activation functions and no bias.
- 216 • Model 3 - Model layers: 33-6-6-1 with linear activation functions.
- 217 • Model 4 - Model layers: 33-6-6-1 with nonlinear (ReLU) activation functions.

218 By comparing the predictive skill of model 1 versus 2 and model 3 versus 4 we can identify
219 the effect of increasing the model complexity from a linear to nonlinear activation functions.
220 This is because the only difference between those two groups is the activation function. Then,
221 separately, we can determine the difference in allowing interdependence between climate modes
222 of variability by comparing the predictive skill of models 1 versus 3 as well as model 2 versus 4.
223 This interdependence is facilitated by either a simple model where each of the 33 neurons in the
224 input layer connects directly with the output layer (as in models 1 and 2), or to connect the input
225 layer to two hidden layers of 6 fully-connected neurons before reaching the output layer.

226 *c. Assessing Predictive Skill*

227 We define that the threshold for our machine learning model to be useful at a given lag
228 time is for its Pearson correlation coefficient for the validation data to exceed persistence. The
229 persistence correlation coefficient in this instance is calculated from the 2-year lowpass filtered
230 regional SIC anomalies lagged between 2 and 20 years, the same lag times as used for our
231 regression analysis. When using the correlation coefficient, it is important to note that, especially
232 at longer lag times, there may be a high correlation between the linear model output and the
233 validation data, but this skill may be present with a smaller amplitude than for the validation data.

234

235 As we do not have sufficiently long periods of observations, we cannot train a separate machine
236 learning model on the observations. Instead, by pooling several regions and SIC anomaly months,
237 we calculate the proportion of positively and negatively correlated modes of variability with
238 the most extreme 10% of SIC positive and negative anomalies. This is not a way of verifying
239 the GCM predictive models per se, rather it shows the range of correlations present within a
240 large ensemble and allows observation to be placed alongside that range. Observations would
241 be expected to typically fall within the large ensemble distribution, but as we do not know how
242 atypical our one realization of reality is, we cannot ascribe meaning to differences from the
243 ensemble mean (Notz 2015). Similarly, when in section e we provide predictions of past and future
244 regional SIC anomalies, good agreement to observations does not explicitly validate our results.

245

246 *d. Sensitivities to time period and forcing*

247 We use a linear detrending for both the SIC and the CVDP variables over the period 1920-2014
248 as this is a simple process to understand and does not make specific assumptions about the
249 time period in question. This is not perfect as the forced response during this period was not
250 entirely linear (see Figure 1 from McBride et al. 2021). This means that some of the very
251 low-frequency variability of the forced response is incorporated into the anomalies of SIC and
252 CVDP variables, rather than being removed by detrending. Therefore, some predictability is
253 due to the shape of the forced response, primarily represented by our input variable of global
254 average surface temperature (TAS), and likely, to a small extent, the SST-derived variables
255 of NINO34, PDO, ATN, AMO, and the IPO. As the simple linear model used in our results
256 considers each variable independently, we can consider TAS similarly to a residual term in
257 the model which does not affect the conclusions we draw about other modes of variability.

258

259 To verify that our results from the period 1920-2014 are robust to different forcing conditions,
260 we compare results with a more linear forcing scenario for the historical period 1970-2014 and
261 a constant pre-industrial forcing scenario. For the 1970-2014 time period the global surface
262 temperature and sea ice area trends are both highly linear (Notz and Stroeve 2016; McBride et al.

263 2021). Consequently, we find that the linear response to TAS in our models is far smaller than in
264 1920-2014 (see Figure S1, compared with Figure 4). The 1970-2014 time period only uses 24
265 years of data (compared with 74 for 1920-2014) and hence the linear response is much more noisy
266 than for 1920-2014 and infrequently exceeds persistence. Therefore, although we get a broadly
267 similar linear responses for each climate mode, the low skill and erratic results mean we cannot
268 use this time period. Pre-industrial control runs (of which 35 GCMs are available to provide
269 222 training years) use constant 1850 forcing and hence TAS trends are near zero over a 74-year
270 time periods. The influence of TAS is indeed found to be much smaller than for 1920-2014
271 (see Figure S2 compared with Figure 4). Very similar linear coefficients to the 1920-2014 time
272 period are found, and are much less erratic and higher skill than the 1970-2014 time period,
273 likely due an order of magnitude more training data. However, the pre-industrial control results
274 provide much smaller linear responses, likely due to the 1850 mean-state exhibiting less variability
275 than the 21st century, due to the long-term thinning of the Arctic sea ice (Kwok and Rothrock
276 2009). We therefore use the 1920-2014 time period, despite the TAS nonlinearity, as it both
277 captures similar SIC variability to the present day and enables the use of sufficient training data.

278

279 **3. Results**

280 *a. A simple linear model captures drivers of low-frequency variability*

281 Predictions of regional low-frequency Arctic sea ice concentration anomalies can be produced
282 from climate modes of variability using a linear model, which are skillful when compared with
283 persistence. In general, we find that the simple linear variant of the machine learning models
284 (model 1) produces the highest predictive skill of the four models across GCMs, regions and
285 seasons. When validating our linear model we find it generally exceeds the skill from persistence
286 for lead times beyond approximately 4 years, but is dependent on the GCM (see Figure 2 for the
287 Chukchi Sea in September). The highest predictive skill is found at approximately a 5-year lead
288 time when the skill of persistence has decayed close to zero while the skill of the linear model
289 declines more slowly with lead time. This temporal pattern of persistence, as well as the su-

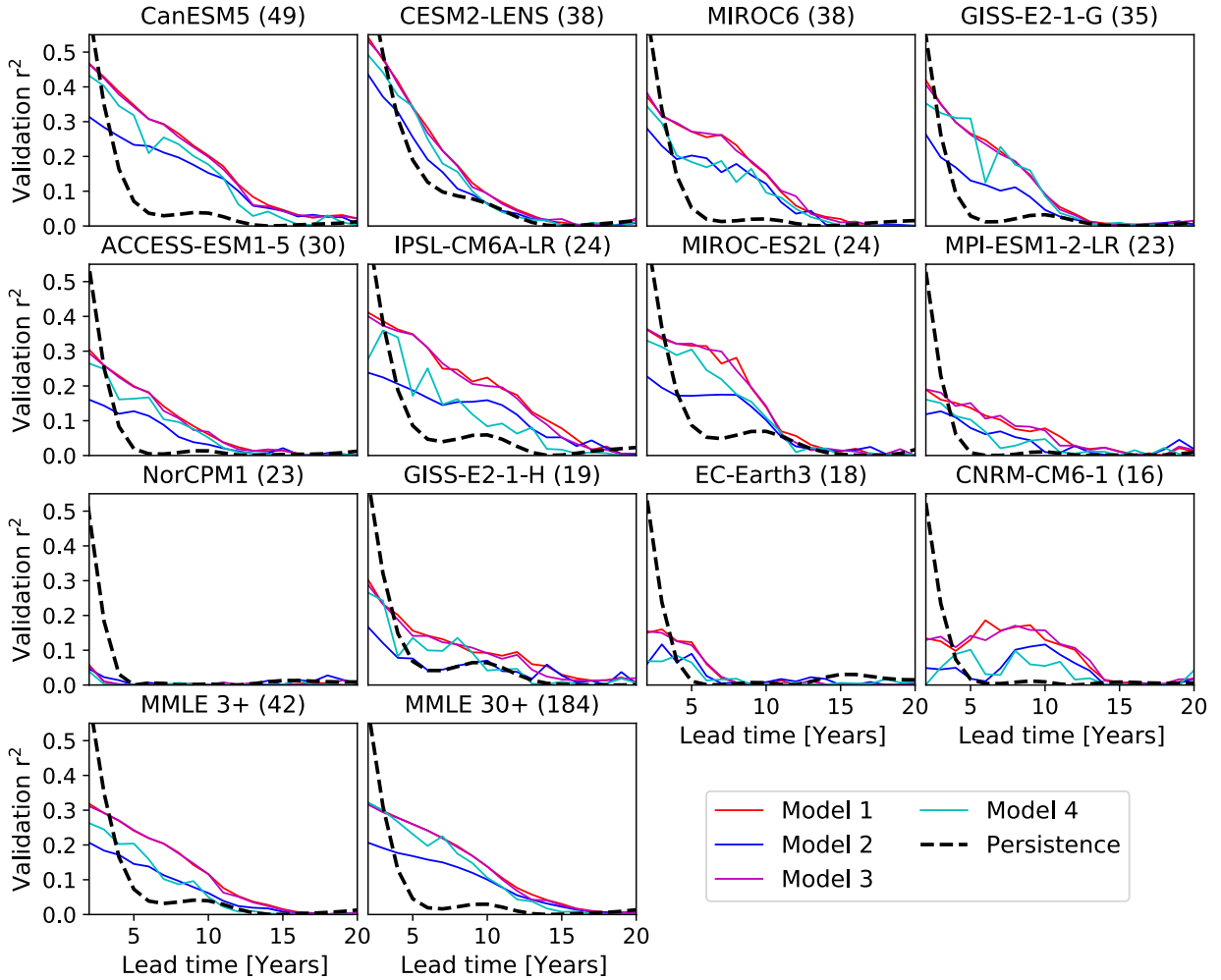
290 periority of the linear model, is found across regions and months with nonzero skill (see section b).
291

292 The simple linear model with no hidden layers (model 1) and the neural network with two
293 hidden layers and linear activation functions (model 3) are nearly identical in their performance
294 across different LEs and MMLEs (see Figure 2). Model 2 with no hidden layers and nonlinear
295 activation functions consistently performs poorly, with model 4 performing similarly to model
296 2 except for LEs and MMLEs with high amounts of training data. The high performance of
297 models 1 and 3 imply that nonlinearities are not required to produce a skillful predictive model.
298 Furthermore, if nonlinearities are included in a model, the nonlinear interactions only become
299 as skillful as the simple linear model at short lead time and with the largest datasets such as
300 the MMLE 30+ which has 184 members used for training. The benefit of including the effect
301 of covariance of climate modes, achieved by including hidden layers in the machine learning
302 model, is not of benefit in our analysis again except in the case of very large training data. In
303 general, we observe a monotonic decline in validation r^2 across the machine learning models,
304 providing the LE or MMLE has sufficiently numerous training members, approximately 30.
305

314 *b. Hotspots of low-frequency variability predictive skill*

315 The summer and autumn marginal seas are generally able to produce the highest skill at a 5-year
316 lead time, however the predictive skill varies considerably between GCM. Based on the MMLE
317 3+, which takes into account the full suite of CMIP6 GCMs with at least 3 ensemble members,
318 the pattern of highest predictability is found in the Beaufort Sea in September, with decaying
319 skill for regions further from the Pacific and for months more distant from September (Figure
320 3). The MMLE 3+ model is unable to produce high predictive skill in the Barents Sea for any
321 season, and the Kara sea appears to have distinct peaks of predictive skill in July and late autumn.
322

323 For models using individual GCMs, the temporal and regional patters of predictive skill are
324 often noisy for neighboring regions and months, unlike the clearer MMLE models. The high
325 predictive skill values of the LEs typically exceed that of the MMLE 3+ for the best regions, but



306 **FIG. 2. The effect of machine learning algorithm complexity on predictive skill.** Pearson correlation
 307 coefficients in the Chukchi Sea in September for the validation data for four machine learning models as shown
 308 for the 12 LEs and 2 MMLE datasets. Model 1 refers to the simple linear model (red), model 2 to the simple
 309 nonlinear model (blue), and Model 3 and Model 4 to the fully-connected 33-6-6-1 neural network with linear
 310 (purple) and nonlinear (cyan) activation functions, respectively. The black dashed line indicates the average
 311 persistence for that lag time for the GCM or GCMs used. Where the model validation r^2 values exceed
 312 persistence the model has predictive skill. Numbers in parentheses indicate the number of ensemble members
 313 used in training.

326 with less coherence between regions and months. Selecting the LE with the highest skill for a
 327 region and month may be appropriate, but each LE's specific spatial and temporal limitations
 328 should be taken into account. The MMLE 3+ has lower predictive skill than the best LEs,

329 but is influenced by all 42 CMIP6 GCMs. Therefore, high predictive skill in the MMLE 3+
330 should be seen as less sensitive to individual GCM biases as it is representative of the general
331 agreement between all GCMs. Some LEs such as CanESM5 and ACCESS-ESM1-5 exhibit
332 unusual patterns of high predictability in the Kara and Chukchi Seas in the winter. Other LEs
333 such as CESM2-LENS, GISS-E2-1-H and MIROC-ES2L have particular regions which are far
334 more predictable than others. For example, the CESM2-LENS simulates high persistence for the
335 Chukchi Sea but not for the Beaufort Sea (see Figure S4 for 5-year persistence) which causes the
336 large disparity in predictive skill between these two regions. As September is of particular interest
337 as the typical minimum annual pan-Arctic sea ice cover, and relatively high validation r^2 values
338 occur across regions for September in the MMLE 3+, this is our focus in subsequent analyses.

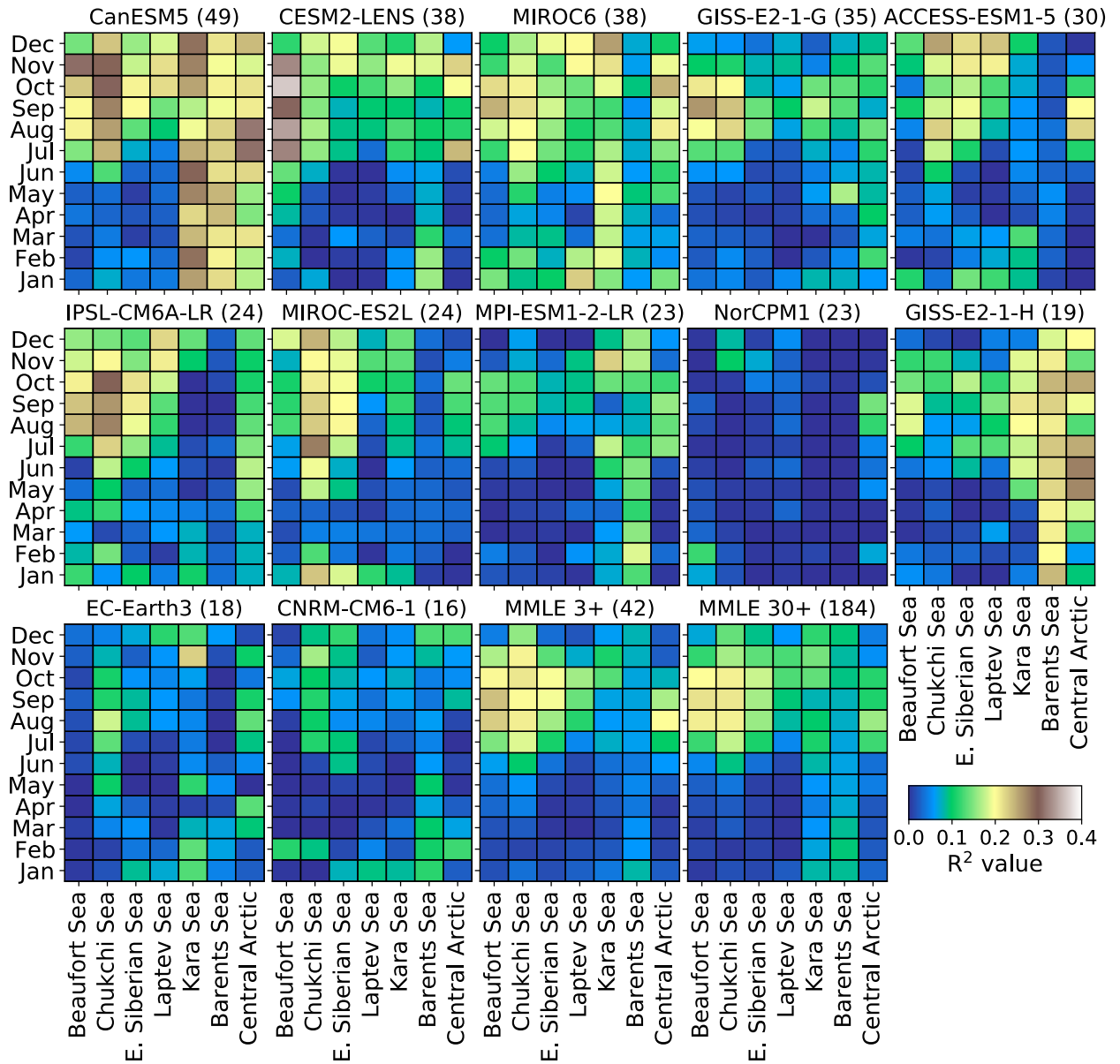
339

345 *c. Linear drivers of regional sea ice anomalies*

346 Using a linear model trained on 42 CMIP6 GCMs (the MMLE 3+ model), we can establish
347 the consensus across GCMs for the independent effect of each mode of variability on regional
348 September SIC anomalies. The lead times where the MMLE 3+ model has no predictive skill is
349 before a 4-year lead time for all regions except the Central Arctic where it is not until a 5-year
350 lag time that the validation r^2 exceeds persistence (see the dotted lines in Figure 4). The most
351 important mode of variability is the IPO, which is strongly positively correlated with the SIC
352 in all regions, especially in the East Siberian and Beaufort Seas (Figure 4). The IPO decays in
353 influence over time, reaching near zero influence on SIC at approximately a 15-year lead time.
354 The global average surface temperature (TAS) also has a very large coefficients, but as this is not a
355 mode of variability and is considered to integrate modes of variability not represented (see section
356 d for a more detailed explanation), we do not discuss in detail the influence of TAS further.

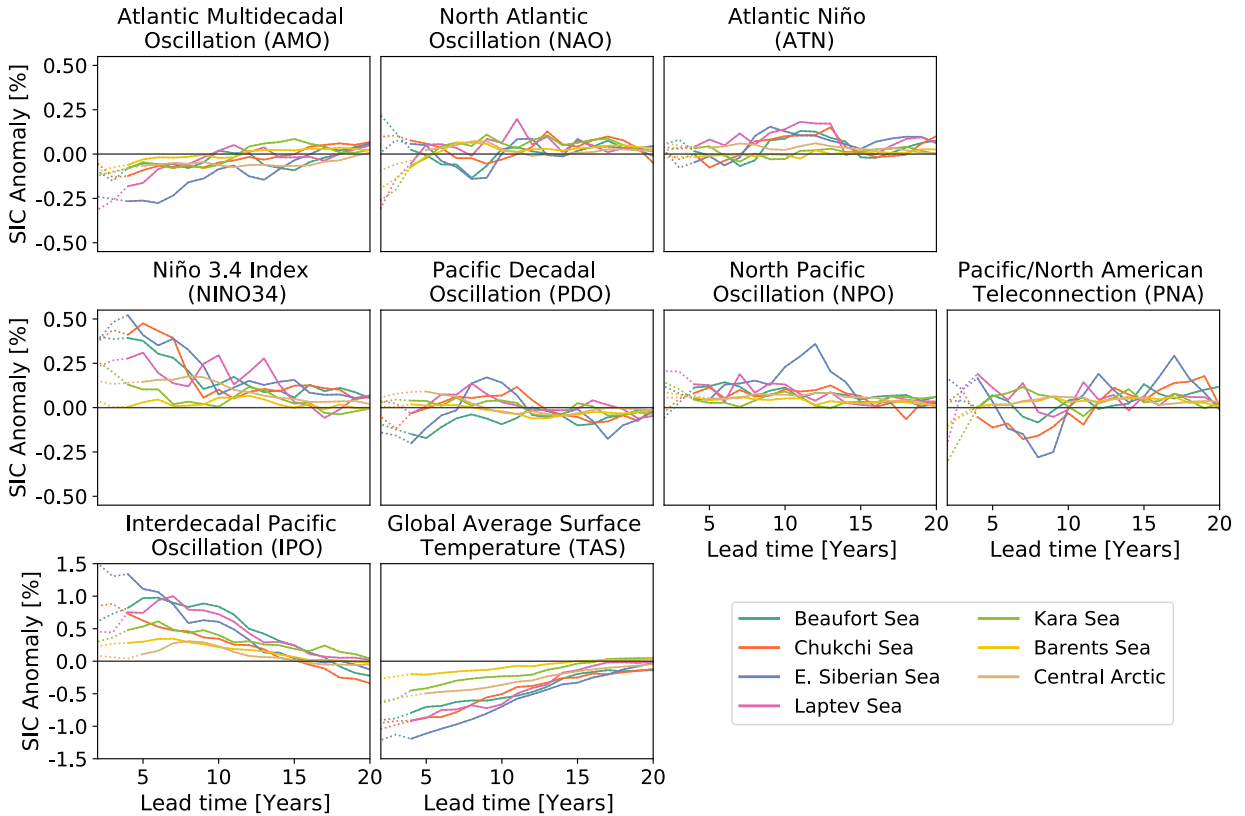
357

366 Aside from the large influence of the IPO, the Niño 3.4 index (NINO34) and the Atlantic
367 Multidecadal Oscillation (AMO) both display a very consistent sign of influence which decays with
368 time. The NINO34 and AMO both have smaller influences than the dominant IPO, approximately
369 one third and one quarter respectively for a given one standard deviation anomaly in each mode



340 FIG. 3. **5-year lagged predictive skill for multiple global climate models and the CMIP6 multi-model**
 341 **ensembles.** Pearson correlation coefficients are shown for the validation data minus persistence at a 5-year lag
 342 time between the input climate modes and sea ice concentration anomalies. Persistence is removed to indicate the
 343 regions and months for each LE or MMLE where predictive skill is high, rather than where explained variability
 344 is high. Numbers in parentheses indicate the total number of ensemble members used for training.

370 of variability. Like the IPO and TAS, the influence of the AMO and NINO34 decays relatively
 371 monotonically with time. As the skill of persistence also declines nearly monotonically, and the
 372 IPO, TAS, NINO34 and AMO all display low-frequency variability, this increases confidence in the



358 **FIG. 4. Linear drivers of September regional sea ice concentration anomalies.** Linear response of a +1
 359 standard deviation anomaly of each of the 8 climate modes and global average surface temperature on sea ice
 360 concentration anomalies in each of the seven Arctic regions. Positive SIC anomaly values indicate a positive
 361 SIC anomaly results from the +1 standard deviation anomaly in the climate mode of variability. The IPO only
 362 provides one annual value, the other climate modes provide seasonal data and the sum of all seasons is shown
 363 here. Solid lines indicate that the validation r^2 value exceeds persistence for a given region and lead time, dashed
 364 lines indicate where there is no predictive skill beyond persistence. Predictive skill occurs for 4- to 20- year lead
 365 times for all regions except for the Central Arctic which has predictive skill for 5- to 20-year lead times.

373 validity of these relationships found in the MMLE 3+. The low-frequency oscillations of the other
 374 sea surface temperature-derived indices of the Pacific Decadal Oscillation (PDO), and to a lesser
 375 extent the Atlantic Niño (ATN), implies the potential for longer-term predictability as with the IPO,
 376 TAS, NINO34 and AMO. However the influence of these modes is small at most time periods and
 377 does not display a monotonic decline with time. This suggests these two modes are not highly im-
 378 portant in driving low-frequency Arctic sea ice variability, but consistency or lack thereof between

379 LEs (see section d) may clarify whether the relationships in the MMLE 3+ are small and indepen-
380 dently consistent in magnitude between GCMs, or small due to disagreement between GCMs.

381

382 The modes of variability based on sea level pressure patterns are generally of a small and highly
383 erratic influence on low-frequency variability of Arctic sea ice. The North Atlantic Oscillation
384 (NAO) and the Pacific/North American Teleconnection (PNA) do have large, regionally distinct
385 effects, on very short time periods. However, their influence decays to near zero at a 4-year
386 lead time which is the threshold for the linear model skill exceeding persistence. At lead
387 times beyond 4 years both modes become erratic and close to zero influence implying they
388 are not important drives of low-frequency variability. The North Pacific Oscillation (NPO)
389 is somewhat less erratic than the NAO and PNA, and its influence remains positive for all
390 regions and time periods. However, as the influence of the NPO is small in magnitude, does
391 not decay with time, and has a suddenly large influence in the East Siberian Sea at a 12-year
392 lead time, this linear driver seems unlikely to be representing a robust physical relationship.

393

394 *d. Low-frequency driver representation across global climate models*

395 Comparing the independent results from 12 LEs aids our interpretation of the linear drivers of
396 SIC anomalies captured in the MMLE 3+. We do this by comparing the datasets for both the
397 medium-term for lead times of 4-9 years (Figure 5a) and the longer-term for lead times of 10-15
398 years (Figure 5b). Although the LE analysis only includes 12 of the 42 GCMs that went into
399 the MMLE 3+ linear model, we can get a sense of the consistency between the CMIP6-suite of
400 GCMs. This informs our interpretation of the two dominant modes of variability, namely the
401 IPO and NINO34 as the LEs are highly consistent in sign for NINO34 but vary considerably
402 for the IPO, for both periods. Although the influence of the IPO is seen to gradually decrease
403 over time for the MMLE 3+, the individual LEs show large magnitudes of influence on SIC for
404 both time periods and the sign is highly inconsistent between LEs. This shows that the positive
405 influence of the NINO34 should be seen as a common feature of CMIP6 GCMs, but there is
406 little consensus regarding the IPO. The strong positive medium-term influence of the IPO in the

407 MMLE 3+ which is larger than the any of the 12 LEs, must therefore be due to the 30 GCMs not
408 part of the 12 LEs. This highlights the importance of taking a multi-model approach for the de-
409 tection of low-frequency variability as two GCMs selected at random may produce opposite results.

410

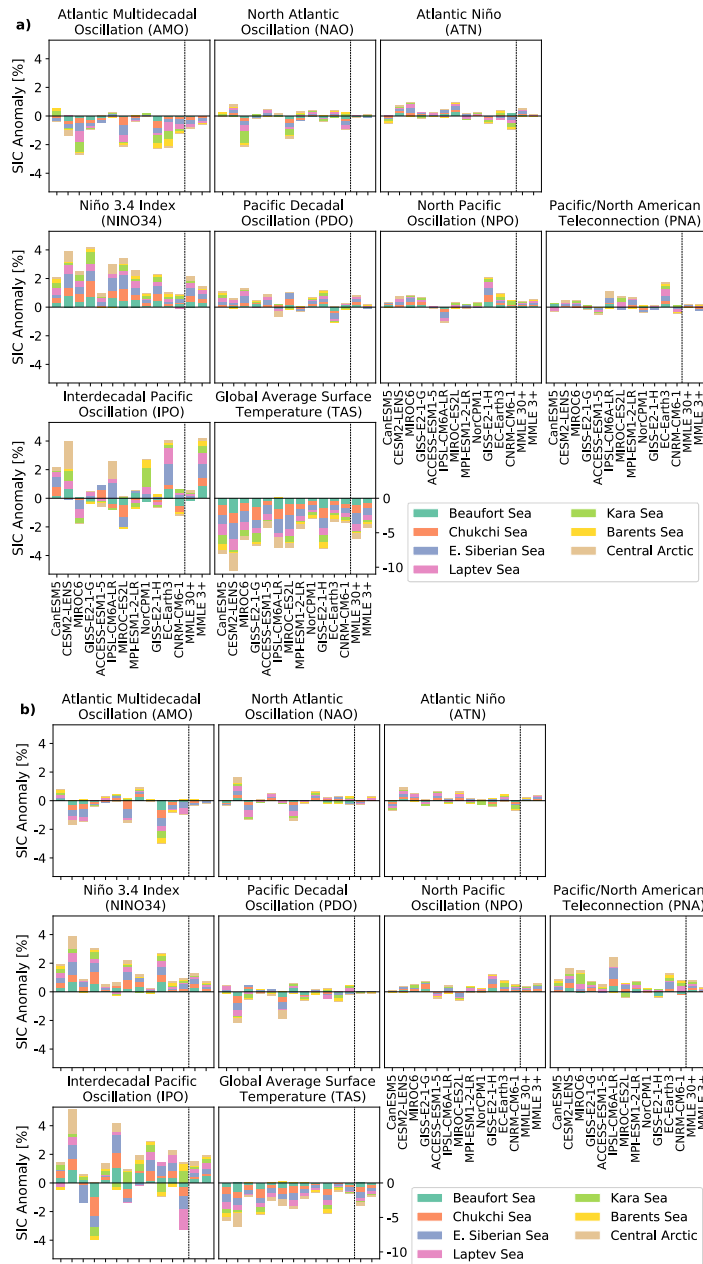
416 The AMO has reasonably good agreement between the LEs with almost all indicating negative
417 influence on regional SIC in the medium-term. For the longer-term, the LEs broadly agree with the
418 sign in the medium-term, although for the full MMLE 3+ the coefficient is near zero due to lower
419 consensus; most but not all of the LEs indicate a large negative value. The PDO in the MMLE 3+
420 has near zero influence for both time periods, by looking at the spread between the LEs we can
421 see that none of the LEs indicate the PDO as being particularly influential and the disagreement
422 in sign further reduces the overall effect for the MMLE 3+. For the other modes of variability
423 we find that almost all of the LEs coefficients are small in magnitude and with little agreement
424 on sign, further indicating that the MMLE 3+ near zero coefficients are a good representation
425 of the CMIP6 consensus of the modes of variability being unimportant at those lead times.

426

427 The average magnitude of influence across all modes of variability differs considerably between
428 individual LEs. For example CESM2-LENS often produces the largest magnitudes for a given
429 mode and NorCPM1 the smallest. Such systematic differences may play out due to differences
430 in the mean state and magnitude of variability by GCM. This may well be the case considering
431 the SIC anomaly is recorded in percentage points and CEMS2-LENS has a low biased summer
432 mean-state (DuVivier et al. 2020) and consequently large variability. Conversely, NorCPM1 has
433 been noted as having a high biased sea ice thickness (Bethke et al. 2021), which may explain
434 why NorCPM1 is an outlier for small low-frequency SIC variability. Again, this indicates
435 care must be taken to understand the effect of limitations to the results from individual LEs.
436 Although many of the CMIP6-suite GCMs are related (Knutti et al. 2013), and their biases may
437 not average out, taking the results from the MMLE 3+ can reduce the risk of extreme outliers.

438

439 Using the remaining ensemble members from our MMLE 3+ trained and validated linear
440 model, we find a wide variety GCMs and members which most closely match the MMLE



411 **FIG. 5. The linear effect on regional SIC for 12 large ensembles and the two multi-model large ensembles.**
 412 Linear response in September sea ice concentration for a +1 standard deviation anomaly of each climate mode,
 413 as in Figure 4, but averaged over two distinct lead times. Bars are the linear response averaged over 4 to 9-year
 414 lead times in a) and 10 to 15-years in b). Agreement within the CMIP6-suite of GCMs is high where bars are
 415 similar in magnitude and sign. Note the different y-axis scale for the global average surface temperature.

441 3+. All of the GCMs listed have equal weighting in training the MMLE 3+, so each test
442 member from all GCMs can be treated equally. There is a large amount of variability between
443 ensemble members from the same GCM (see Figure 6). Additionally CESM2-LENS has far
444 more variation between the micro-perturbations (atmospheric state), than between ensemble
445 members with different ocean states (macro-perturbations) (see Figure S3), as also found
446 by Kay et al. 2022 for pan- Arctic volume variability. This indicates that for a 74-year
447 time period the specific manifestation of the relationships between climate variability modes
448 and regional Arctic SIC anomalies can be highly dependent on the initial climate state.

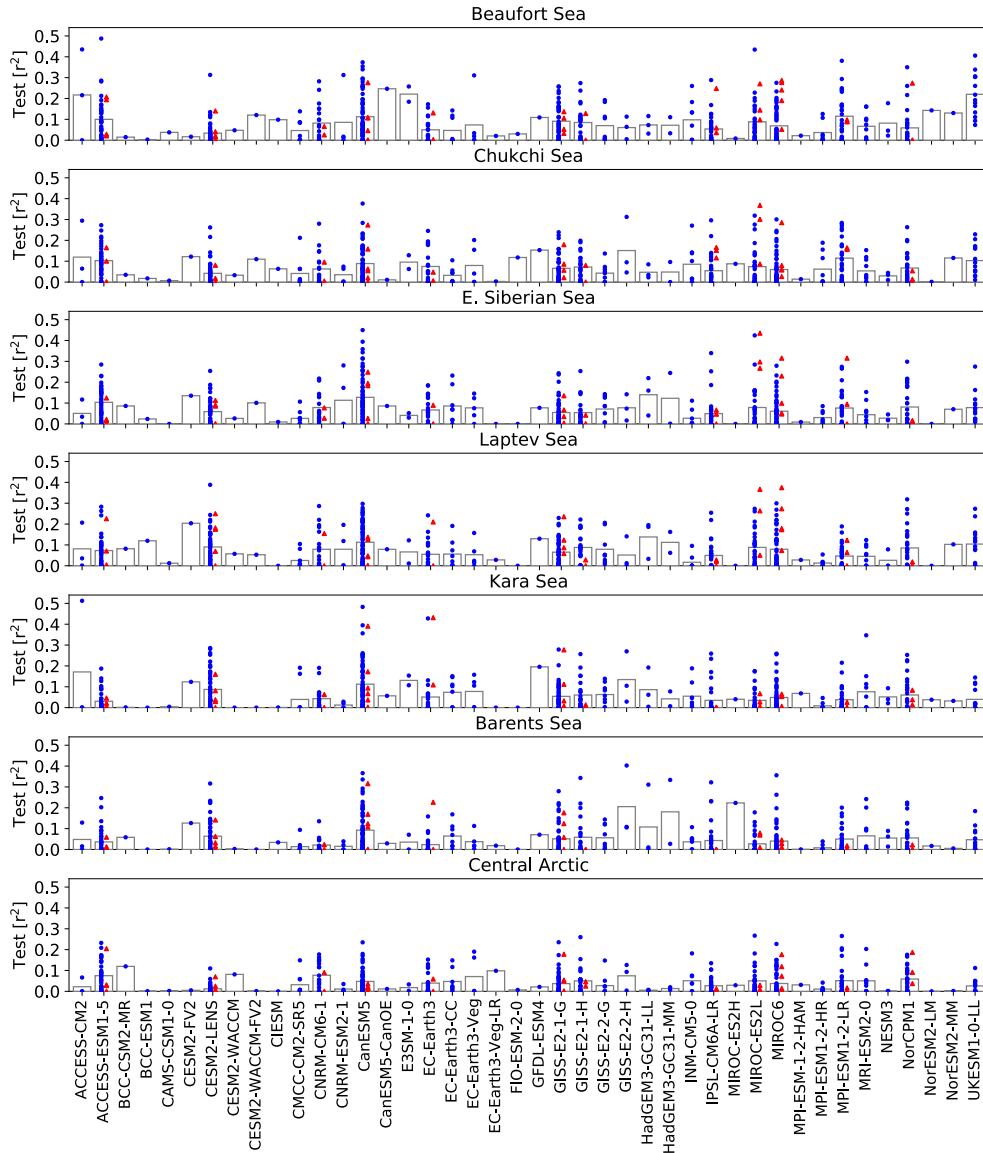
449
450

460 When using the MMLE3+ model on the test members of a given GCM, there are large
461 differences in test r^2 values across the ensemble members. This limits our ability to determine
462 which GCMs are most like the CMIP6 consensus if they have small ensemble sizes which cannot
463 populate the full range of potential values (Notz 2015). Observational comparison with a similar
464 time period will therefore be difficult as observations could be expected, rather unhelpfully, to fall
465 somewhere between 0 and 0.5 r^2 if the actual climate system has relationships like the MMLE
466 3+. However, the MMLE 3+ model appears to be well generalized to multiple GCMs as the test
467 r^2 values appear very similar if a linear model is trained on all 42 GCMs as for the MMLE 3+
468 (blue circles in Figure 6) or only on other members from the same GCM as for the LE (red triangles).

469

470 *e. Observational comparisons*

471 Correlations between the climate modes and extreme SIC anomalies show observations broadly
472 fall within what is simulated for the LEs, but validation is difficult due to the large differences
473 between realizations. In order to directly compare observations with ensemble members, we
474 compute the correlation between the 6 most extreme regional SIC anomaly years in the period
475 1956-2022 and correlate whether each mode of variability was in a positive or negative phase.
476 To make a more representative sample, we pool the seven regions (except the Barents Sea where
477 summer variability is near zero), averaged over a 10- to 15-year lead time. However, the correla-



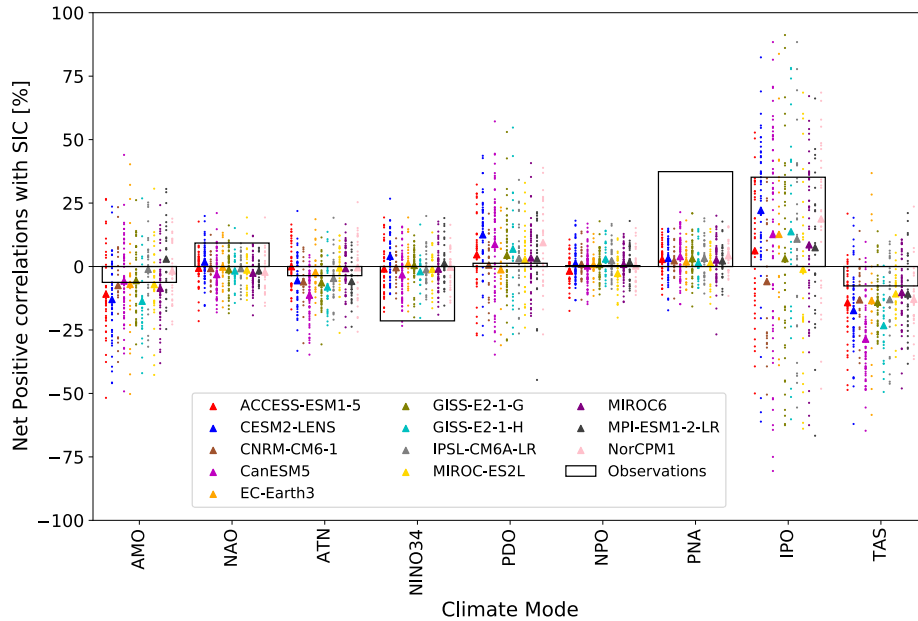
451 FIG. 6. September r^2 values for the test ensemble members from either the multi-model large ensemble
 452 (3+, blue) or the 12 single GCM large ensembles (red). The performance of the test members (third and later
 453 ensemble members) for the 42 GCMs included in the MMLE 3+ model are shown as blue circles, ensemble
 454 mean values are indicated by gray bars. The red triangles indicate the performance of the test members for the
 455 individually trained linear models for each of the 12 LEs, where 10% of the LE members were reserved for
 456 testing against the linear model trained and validated on the first 75% and 15% of members from each GCM.
 457 Where the red triangles and blue circles for a given GCM have a similar distribution, the MMLE 3+ is equally
 458 good at capturing the relationships between climate modes and SIC as the LE, indicating the MMLE 3+ is well
 459 generalized. The r^2 values are for a 5-year lead time minus persistence.

478 tions should not be seen as comparable to the linear model as each season is weighted equally and
479 the correlations are binary, unlike the abilities of the linear model which applies lower weights
480 to less important seasons and has a continuous rather than binary representation of relationships.
481 Observations fall within the ensemble spread for all modes of variability except for the PNA for all
482 LEs and NINO34 for all LEs except CanESM5 (see Figure 7). This suggests that the observations
483 and GCMs match well in terms of the influence of modes of variability on regional SIC anomalies,
484 except for the PNA and NINO34. As NINO34 is a large contribution to regional SIC anomalies
485 in the LE and MMLE 3+ linear models, the far stronger correlation of observations may mean in
486 our one realization of reality the NINO34 index has played a larger role than simulated in many
487 climate models. Again, the large spread between realizations within a large ensemble highlights
488 the extremely large range that observations would be expected to fall within (particularly for the
489 IPO), and hence the difficulty of validating the simulated low-frequency drivers with observations.
490

499 *f. Future projections*

500 Our limited time period of observations may not be representative of a typical climate
501 realization and therefore may arbitrarily match well or poorly to a specific machine learning
502 model trained on GCMs. However, validation of our LE and MMLE 3+ models against the
503 period 1956-2022 may have some implications for how well we can expect projections over the
504 next 4-20 years to hold up. The r^2 values of the MMLE 3+ validated against the observations
505 (Figure 8 prediction columns) is similar to that of the MMLE 3+ validated against the second
506 large ensemble members (Figure 3). The MMLE 3+ and the best LEs when used for hindcasting
507 SIC anomalies from observed climate modes, often achieve r^2 values of between 0.2-0.4 above
508 persistence, but is highly regionally dependent. As the MMLE 3+ typically has the highest or near
509 highest validation skill against the observations, we use these for future projections in the following.
510

520 For all regions of the Arctic, our linear model predicts below trend sea ice concentrations
521 over the coming decade. The seven regions have different time evolutions of the projected
522 SIC anomalies, however all regions for the MMLE 3+ projections show accelerated SIC loss



491 **FIG. 7. Correlations between ensemble members and observations between modes of variability and**
 492 **extreme SIC anomaly events.** The 6 most extreme SIC positive and negative anomalies are found for each
 493 ensemble member and September observations over the period 1956-2014. For a lead time of 10-15 years the
 494 positive and negative correlations with each mode of variability is summed. These data are the average for the
 495 Beaufort, Chukchi, East Siberian, Kara and Laptev Seas and the Central Arctic. Each colored dot indicates the
 496 correlations for a single ensemble member, with the same colored triangle indicating the ensemble mean. The
 497 observed value for each variable is shown with a black hollow bar. When observations lie within a given GCM
 498 ensemble member distribution, the correlation in the observations is consistent with that simulated in the GCM.

523 due to low-frequency variability over the 20 years following 2022 (see Figure 8). Taking the
 524 pan-Arctic as a whole, the predicted negative anomaly from the linear trend is the largest anomaly
 525 at a 5-year lead time during the period 1956-2022. Therefore, our MMLE 3+ model predicts
 526 current climate modes as being particularly conducive to a large low-frequency SIC anomaly.
 527 This is fairly consistent across LEs, with the only large outlier being the CESM2-LENS which
 528 predicts an extreme accelerated loss due to being a large outlier in Central Arctic projections.
 529 This outlier is likely due to thin biased ice as discussed in section d. Comparing the persistence
 530 of CESM2-LENS with CESM2-lessmelt runs which have thicker sea ice (Kay et al. 2022), the
 531 lessmelt CESM2 variant is more in line with the persistence in other GCMs (see Figure S4).

532 This indicates the low thickness bias likely caused the enhanced simulated variability outlier.

533

534 The contributions to this predicted accelerated SIC loss throughout the Arctic in the coming
535 decade is dominated by the large negative anomalies in 2022 in both the IPO and NINO34 and the
536 positive phase of the AMO. Furthermore, the above trend surface temperature warming in 2022 is
537 also modeled as being a large contribution in the year 2027 (see Figure 8q,r). Only the negative
538 phase of the PDO in 2022 is expected to counter the accelerated sea ice loss by leading to positive
539 SIC anomalies in the Pacific sector. The remaining modes of variability are either in near neutral
540 phase in 2022 or have small influences on the linear model and hence do not feature as contributing
541 to future anomalies. The alignment of modes of variability phases in 2022 combine to simulate a
542 negative anomaly to the linear trend larger than any anomaly predicted during the period 1956-2021.

543

544

545 **4. Discussion**

546 The quantity and quality of GCM data available from CMIP6 simulations is unprecedented
547 (Davy and Outten 2020), allowing us to investigate whether nonlinearities and climate mode
548 covariance is essential to produce skillful SIC projections. The fact that linear relationships were
549 found to be sufficient for skillful projections shows promise for using the dominant modes of
550 variability we identified of the IPO, NINO34 and the AMO. Nonlinearities and covariance in
551 the effect of climate modes on Arctic sea ice is likely to exist (e.g. Heo et al. 2021), but may
552 require additional data or more prescriptive methods to improve skill beyond that by achieved
553 using simple linear relationships. By using 42 GCMs in our MMLE 3+ linear model, we
554 did not degrade our skill when compared with training our linear model on a single GCM
555 (see section d). This shows that a generalized linear model can be obtained from a variety
556 of GCMs differing in model physics, model biases and ocean states, but that this generalized
557 linear model still has a large range of predictive skill outcomes dependent on realization.

558

559

560 Previous studies have primarily focused on seasonal or interannual timescales of variability, with
561 the notable exceptions of the IPO and AMO which have been considered on decadal timescales.
562 We found the IPO to be the most influential mode of variability on all lead times between 4 and
563 20 years. In previous research the IPO has not featured except as found by Screen and Deser 2019
564 for the GCM CESM1-LE. This agreed with the positive correlation in our MMLE 3+ linear model
565 that was strongest in the CESM2-LENS large ensemble. The moderate disagreement in sign and
566 longevity of the IPO's influence on SIC in CMIP6 LEs follows on from research that CMIP5
567 GCMs generally poorly simulate the effect of the IPO (Baxter et al. 2019; Ding et al. 2019; Topál
568 et al. 2020). In addition to the lack of consensus between GCMs broadly, the correlation appears
569 highly sensitive to realization (see Figure 7). Additional focus on this mode with a wider variety of
570 modeling applications appears needed and is particularly pressing given the strong current negative
571 phase (see Figure 8q). The AMO was found in our MMLE 3+ linear model to be negatively
572 correlated with all regions of the Arctic sea ice, which shows good agreement with previous
573 studies (e.g. Day et al. 2012; Miles et al. 2014; Li et al. 2018b) for the pan-Arctic or Atlantic
574 sector on decadal timescales. However, the AMO itself may have a forced component (Murphy
575 et al. 2021; Klavans et al. 2022), and its oscillatory timescale varies considerably between GCMs
576 (Lee et al. 2021), potentially limiting the use of the AMO as an independent variable. However,
577 the fact that the pre-industrial control simulations (see Figure S2) match well with the MMLE 3+
578 for 1920-2014 for the AMO, IPO and NINO34 suggests that forcing context is not highly important.

579
580 El Niño and La Niña have been shown to be influential on Arctic sea ice and generally suggest
581 that NINO34 is positively correlated with SIC except for the Beaufort Sea (e.g. Clancy et al. 2021;
582 Hu et al. 2016; Jeong et al. 2022b). However, the lead times considered previously were shorter
583 than our 4-20 year timescale, making our positively correlated influence hard to directly compare
584 with previous research. Furthermore, previous literature on shorter timescales have noted the
585 importance of the type of El Niño regime (Jeong et al. 2022a; Lee et al. 2023) and the likely
586 nonlinear climate response from NINO34 (Hoerling et al. 1997). The PDO was previously not
587 found to be highly important by itself (Zhang et al. 2020) and its weak influence may also have
588 changed over time (Kim et al. 2020); similarly we also only found a small influence of the PDO.
589 The ATN is the only negligible mode of variability derived from SSTs, but has not previously

590 been identified as specific driver of Arctic sea ice variability. However the tropical Atlantic was
591 been suggested to influence Arctic sea ice (Meehl et al. 2018), hence the unimportant nature
592 of the ATN does not preclude other aspects of tropical Atlantic being important. Consistent
593 with the previous lack of evidence of influence beyond interannual timescales, the sea level
594 pressure-derived modes of variability (the NAO, NPO and PNA) were found to have negligible
595 effect at lead times of 4-20 years. Previous research has shown the effect of the NAO to decay to
596 zero after approximately 2 years (Ukita et al. 2007), this timescale and the regional correlations
597 (e.g. Serreze et al. 2007; Döscher et al. 2010) align with our findings given the smoothing inherent
598 in our lowpass filtered data. This provides confidence in our linear model's ability to capture
599 higher frequency variability but dismiss low-frequency influence from these modes of variability.

600

601 **5. Conclusions**

602 We have shown that low-frequency variability of regional Arctic sea ice can be modeled using
603 linear drivers consisting of climate modes of variability. We achieve predictions superior to
604 persistence for most regions for a lead time of 4-20 years and find that the climate modes of
605 variability can be considered independently without reducing skill. By comparing the linear
606 responses between twelve large ensembles from CMIP6 and a multi-model large ensemble
607 comprising of 42 GCMs, we find where there is consensus of the dominant linear drivers
608 of low-frequency sea ice variability except in the case of the Interdecadal Pacific Oscillation
609 (IPO). In the pan-Arctic we are able to explain up to 58% of observed low-frequency sea ice
610 concentration variability at lead times of 5 years. However, the ability of a GCM or a multi-model
611 large ensemble to predict unseen ensemble members or observations can vary wildly depending
612 on the realization of internal variability. Hence, this both complicates the analysis of small
613 samples of GCMs and the application and verification of these relationships with observations.

614

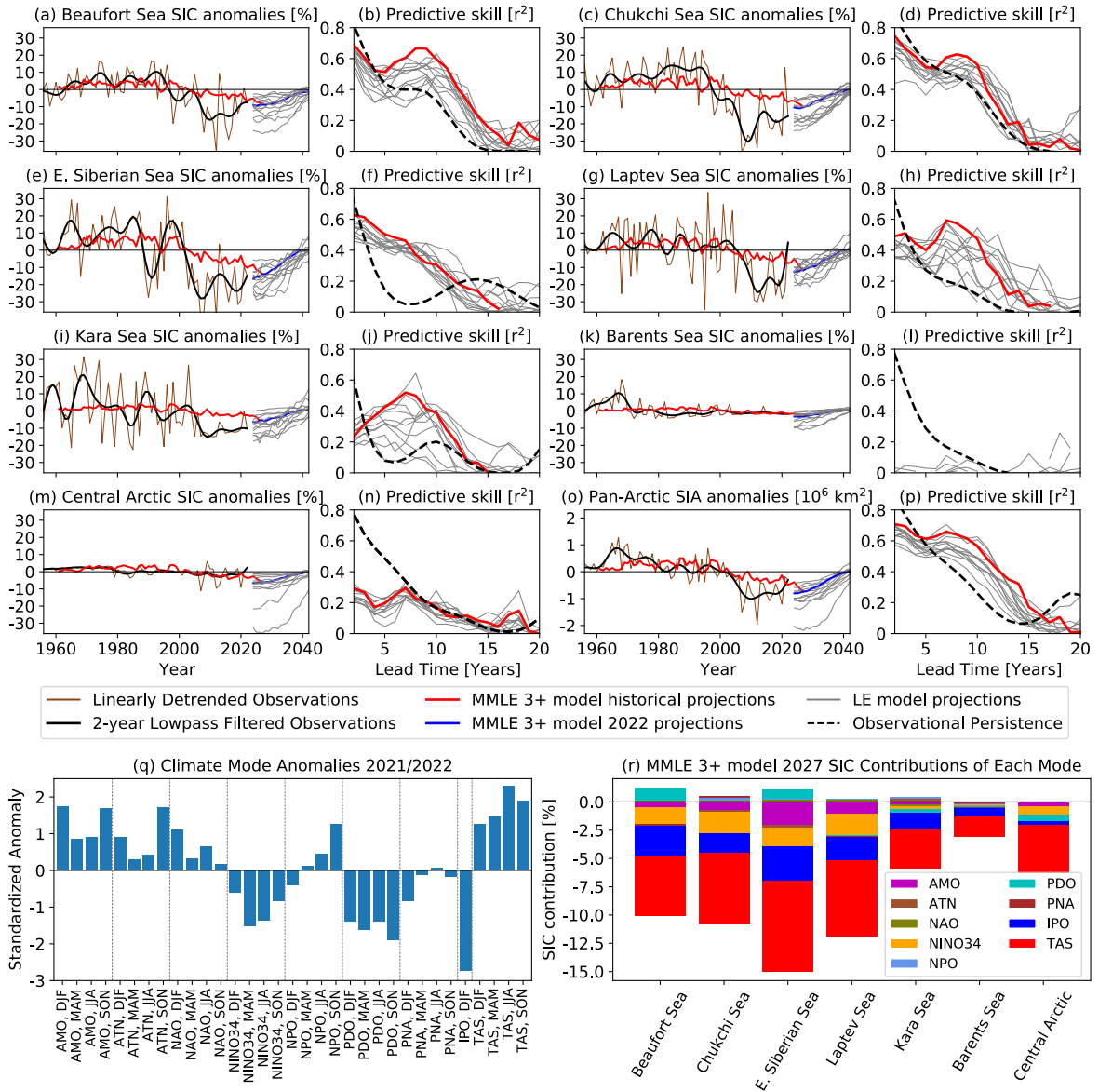
615 The most important modes of variability we found were the IPO, Nino 3.4 Index (NINO34)
616 and the Atlantic Mutidecadal Oscillation (AMO). The multi-model large ensemble linear
617 model showed the IPO to have a strong positive correlation with this being most pronounced

618 in the East Siberian, Beaufort and Laptev Seas at lead times of up to 14 years. Although
619 this large magnitude of influence of the IPO was found across GCMs, the sign and regional
620 influence was especially dependent on the GCM used and the specific realization of internal
621 variability. NINO34 was found to be positively correlated with SIC anomalies in all regions,
622 particularly in the Pacific sector. This correlation was robust between GCMs, but disagreement
623 occurred regarding the longevity of this positive correlation. The AMO was the only other
624 mode of variability considered important for long periods of time, being modeled as highly
625 negatively correlated with SIC across all regions for up to approximately 10 years. How-
626 ever, the agreement across CMIP6 GCMs for the AMO was less consistent than NINO34.

627

628 When using our linear model to make predictions, we find a near 'perfect storm' of modes of
629 variability in the year 2021/2022 to induce an acceleration to the sea ice loss trend over the next
630 decade. The primary influences of this projected acceleration of low-frequency variability driven
631 sea ice loss are an above trend global average surface temperature warming, a negative IPO, La Niña
632 conditions, and a positive AMO. For the pan-Arctic, the projected low-frequency deviation from the
633 long-term trend due to current climate mode phase configurations is expected to be the largest since
634 at least 1956. Of course, the sea ice anomalies that will actually be observed are still dominated by
635 interannual variability, which makes up roughly three quarters of the total variability. Thus, while
636 we cannot say with confidence that a new record low September extent will occur over the next
637 decade, the modeled low-frequency variability suggests that extreme low SIC values will be more
638 likely over the coming decade, as they will enhance rather than oppose the long-term negative trend.

639



511 **FIG. 8. Linear model projections of SIC anomalies based on observed climate modes.** The projection
 512 subplots a,c,e,g,i,k,m,o show the observed 1956-2022 regional or pan-Arctic SIC anomalies (brown), the 2-year
 513 lowpass filtered anomalies (black), the MML3+ linear model historical hindcasts on a 5-year lead time (red),
 514 and the future projections based on the climate mode anomalies observed in 2022 (or 2021 for the SON season)
 515 using the MMLE 3+ (blue) and individual LEs (grey). The prediction skill subplots b,d,f,h,j,l,n,p show the
 516 observed persistence in dashed back lines while the MMLE 3+ and LE hindcast performances for 1976-2022
 517 at 2- to 20- year lead times are shown in red and gray respectively. The subplot q depicts the observed climate
 518 mode anomalies for the year 2022 (or 2021 for season SON). Subplot r shows the MMLE 3+ contribution to the
 519 projected anomalies in 2027 based on 2022 data of each of the modes of variability.

640 *Acknowledgments.* This work was supported by the National Science Foundation under grant
641 number 1847398. A. Jahn's contribution was also supported by an Alexander von Humboldt
642 fellowship. We would also like to acknowledge high-performance computing on Cheyenne
643 (doi:10.5065/D6RX99HX) provided by NCAR's Computational and Information Systems Lab-
644 oratory, sponsored by the National Science Foundation. Further, we thank Adam Philips for
645 processing updates to the Climate Variability Diagnostics Package output used in this analysis. We
646 also thank Libby Barnes and David Hall for useful conversations in the early part of the project.

647 *Data availability statement.* The data used in this study is freely available at [https://esgf-](https://esgf-node.llnl.gov/projects/cmip6/)
648 [node.llnl.gov/projects/cmip6/](https://esgf-node.llnl.gov/projects/cmip6/) for the CMIP6 global climate model data except for the CESM2-
649 LENS, which is available at <https://www.cesm.ucar.edu/community-projects/lens2/data-sets>. The
650 CVDP data is available at <https://www.cesm.ucar.edu/projects/cvdp/data-repository>. The observa-
651 tional sea ice concentration data is freely available from <https://nsidc.org/data/g02202/versions/4>.
652 Upon publication, all code required to replicate this study will be made open-access at Zenodo,
653 currently it is available at <https://github.com/chrisrwp/low-frequency-variability>. Additionally the
654 linear model coefficients and the observational CVDP output data processed for this analysis will
655 be made available at the Arctic Data Center upon acceptance of this manuscript.

656 **References**

- 657 Bader, D. C., R. Leung, M. Taylor, and R. B. McCoy, 2019: E3SM-Project E3SM1.0 model
658 output prepared for CMIP6 CMIP historical. Earth System Grid Federation, [https://doi.org/](https://doi.org/10.22033/ESGF/CMIP6.4497)
659 [10.22033/ESGF/CMIP6.4497](https://doi.org/10.22033/ESGF/CMIP6.4497).
- 660 Barnes, E. A., J. W. Hurrell, I. Ebert-Uphoff, C. Anderson, and D. Anderson, 2019: Viewing
661 Forced Climate Patterns Through an AI Lens. *Geophysical Research Letters*, **46**, 13 389–13 398,
662 <https://doi.org/10.1029/2019GL084944>.
- 663 Barnhart, K. R., C. R. Miller, I. Overeem, and J. E. Kay, 2016: Mapping the future expansion of
664 Arctic open water. *Nature Climate Change*, **6**, 280–285, <https://doi.org/10.1038/nclimate2848>.
- 665 Baxter, I., and Coauthors, 2019: How tropical Pacific surface cooling contributed to accelerated
666 sea ice melt from 2007 to 2012 as ice is thinned by anthropogenic forcing. *Journal of Climate*,
667 **32 (24)**, 8583–8602, <https://doi.org/10.1175/JCLI-D-18-0783.1>.
- 668 Bentsen, M., and Coauthors, 2019: NCC NorESM2-MM model output prepared for CMIP6 CMIP
669 historical. Earth System Grid Federation, <https://doi.org/10.22033/ESGF/CMIP6.8040>.
- 670 Bethke, I., and Coauthors, 2019: NCC NorCPM1 model output prepared for CMIP6 CMIP
671 historical. Earth System Grid Federation, <https://doi.org/10.22033/ESGF/CMIP6.10894>.
- 672 Bethke, I., and Coauthors, 2021: NorCPM1 and its contribution to CMIP6 DCP. *Geoscientific*
673 *Model Development*, **14**, 7073–7116, <https://doi.org/10.5194/gmd-14-7073-2021>.
- 674 Blanchard-Wrigglesworth, E., K. C. Armour, C. M. Bitz, and E. Deweaver, 2011: Persistence
675 and inherent predictability of Arctic sea ice in a GCM ensemble and observations. *Journal of*
676 *Climate*, **24**, 231–250, <https://doi.org/10.1175/2010JCLI3775.1>.
- 677 Blanchard-Wrigglesworth, E., and M. Bushuk, 2019: Robustness of Arctic sea-ice predictability
678 in GCMs. *Climate Dynamics*, **52**, 5555–5566, <https://doi.org/10.1007/s00382-018-4461-3>.
- 679 Bonan, D. B., and E. Blanchard-Wrigglesworth, 2020: Nonstationary teleconnection between
680 the pacific ocean and arctic sea ice. *Geophysical Research Letters*, **47**, e2019GL085 666,
681 <https://doi.org/10.1029/2019GL085666>.

- 682 Bonan, D. B., M. Bushuk, and M. Winton, 2019: A spring barrier for regional predictions of
683 summer arctic sea ice. *Geophysical Research Letters*, **46**, 5937–5947, [https://doi.org/10.1029/](https://doi.org/10.1029/2019GL082947)
684 2019GL082947.
- 685 Bonan, D. B., F. Lehner, and M. M. Holland, 2021: Partitioning uncertainty in projections of
686 Arctic sea ice. *Environmental Research Letters*, **16**, <https://doi.org/10.1088/1748-9326/abe0ec>.
- 687 Boucher, O., and Coauthors, 2018: IPSL IPSL-CM6A-LR model output prepared for CMIP6
688 CMIP historical. Earth System Grid Federation, <https://doi.org/10.22033/ESGF/CMIP6.5195>.
- 689 Brown, J. R., and Coauthors, 2020: Comparison of past and future simulations of ENSO in
690 CMIP5/PMIP3 and CMIP6/PMIP4 models. *Climate of the Past*, **16**, 1777–1805, [https://doi.org/](https://doi.org/10.5194/cp-16-1777-2020)
691 10.5194/cp-16-1777-2020.
- 692 Bushuk, M., and D. Giannakis, 2017: The seasonality and interannual variability of Arctic Sea ice
693 reemergence. *Journal of Climate*, **30**, 4657–4676, <https://doi.org/10.1175/JCLI-D-16-0549.1>.
- 694 Bushuk, M., R. Msadek, M. Winton, G. Vecchi, X. Yang, A. Rosati, and R. Gudgel, 2019: Regional
695 arctic sea–ice prediction: potential versus operational seasonal forecast skill. *Climate Dynamics*,
696 **52**, 2721–2743, <https://doi.org/10.1007/S00382-018-4288-Y/FIGURES/11>.
- 697 Cao, J., and B. Wang, 2019: NUIST NESMv3 model output prepared for CMIP6 CMIP historical.
698 Earth System Grid Federation, <https://doi.org/10.22033/ESGF/CMIP6.8769>.
- 699 Clancy, R., C. Bitz, and E. Blanchard-Wrigglesworth, 2021: The Influence of ENSO on Arctic Sea
700 Ice in Large Ensembles and Observations. *Journal of Climate*, **34**, 9585–9604, [https://doi.org/](https://doi.org/10.1175/JCLI-D-20-0958.1)
701 10.1175/JCLI-D-20-0958.1.
- 702 Crawford, A., J. Stroeve, A. Smith, and A. Jahn, 2021: Arctic open-water periods are projected
703 to lengthen dramatically by 2100. *Communications Earth and Environment*, **2**, [https://doi.org/](https://doi.org/10.1038/s43247-021-00183-x)
704 10.1038/s43247-021-00183-x.
- 705 Danabasoglu, G., 2019a: NCAR CESM2-FV2 model output prepared for CMIP6 CMIP historical.
706 Earth System Grid Federation, <https://doi.org/10.22033/ESGF/CMIP6.11297>.
- 707 Danabasoglu, G., 2019b: NCAR CESM2 model output prepared for CMIP6 CMIP historical.
708 Earth System Grid Federation, <https://doi.org/10.22033/ESGF/CMIP6.7627>.

- 709 Danabasoglu, G., 2019c: NCAR CESM2-WACCM-FV2 model output prepared for CMIP6 CMIP
710 historical. Earth System Grid Federation, <https://doi.org/10.22033/ESGF/CMIP6.11298>.
- 711 Danabasoglu, G., 2019d: NCAR CESM2-WACCM model output prepared for CMIP6 CMIP
712 historical. Earth System Grid Federation, <https://doi.org/10.22033/ESGF/CMIP6.10071>.
- 713 Davy, R., and S. Outten, 2020: The Arctic surface climate in CMIP6: Status and developments
714 since CMIP5. *Journal of Climate*, **33**, 8047–8068, <https://doi.org/10.1175/JCLI-D-19-0990.1>.
- 715 Day, J. J., J. C. Hargreaves, J. D. Annan, and A. Abe-Ouchi, 2012: Sources of multi-decadal
716 variability in Arctic sea ice extent. *Environmental Research Letters*, **7**, <https://doi.org/10.1088/1748-9326/7/3/034011>.
- 718 Day, J. J., E. Hawkins, and S. Tietsche, 2014: Will Arctic sea ice thickness initialization improve
719 seasonal forecast skill? *Geophysical Research Letters*, **41** (21), 7566–7575, <https://doi.org/10.1002/2014GL061694>.
- 721 Deser, C., and Coauthors, 2020: Insights from Earth system model initial-condition large en-
722 sembles and future prospects. *Nature Climate Change*, **10**, 277–286, <https://doi.org/10.1038/s41558-020-0731-2>.
- 724 Ding, Q., and Coauthors, 2019: Fingerprints of internal drivers of Arctic sea ice loss in ob-
725 servations and model simulations. *Nature Geoscience*, **12**, 28–33, <https://doi.org/10.1038/s41561-018-0256-8>.
- 727 Dix, M., and Coauthors, 2019: CSIRO-ARCCSS ACCESS-CM2 model output prepared for CMIP6
728 CMIP historical. Earth System Grid Federation, <https://doi.org/10.22033/ESGF/CMIP6.4271>.
- 729 Docquier, D., T. Koenigk, R. Fuentes-Franco, M. P. Karami, and Y. Ruprich-Robert, 2021: Impact
730 of ocean heat transport on the Arctic sea-ice decline: a model study with EC-Earth3. *Climate
731 Dynamics*, **56**, 1407–1432, <https://doi.org/10.1007/s00382-020-05540-8>.
- 732 Döscher, R., K. Wyser, H. E. Meier, M. Qian, and R. Redler, 2010: Quantifying Arctic contributions
733 to climate predictability in a regional coupled ocean-ice-atmosphere model. *Climate Dynamics*,
734 **34** (7), 1157–1176, <https://doi.org/10.1007/s00382-009-0567-y>.

735 DuVivier, A. K., M. M. Holland, J. E. Kay, S. Tilmes, A. Gettelman, and D. A. Bailey, 2020:
736 Arctic and Antarctic Sea Ice Mean State in the Community Earth System Model Version 2
737 and the Influence of Atmospheric Chemistry. *Journal of Geophysical Research: Oceans*, **125**,
738 <https://doi.org/10.1029/2019JC015934>.

739 Dörr, J., D. B. Bonan, M. Årthun, L. Svendsen, and R. C. J. Wills, 2023: Forced and internal
740 components of observed arctic sea-ice changes. *The Cryosphere Discuss.*, [https://doi.org/10.](https://doi.org/10.5194/tc-2023-29)
741 [5194/tc-2023-29](https://doi.org/10.5194/tc-2023-29).

742 EC-Earth-Consortium, 2019a: EC-Earth-Consortium EC-Earth3 model output prepared for
743 CMIP6 CMIP historical. Earth System Grid Federation, [https://doi.org/10.22033/ESGF/CMIP6.](https://doi.org/10.22033/ESGF/CMIP6.4700)
744 [4700](https://doi.org/10.22033/ESGF/CMIP6.4700).

745 EC-Earth-Consortium, 2019b: EC-Earth-Consortium EC-Earth3-Veg model output prepared for
746 CMIP6 CMIP historical. Earth System Grid Federation, [https://doi.org/10.22033/ESGF/CMIP6.](https://doi.org/10.22033/ESGF/CMIP6.4706)
747 [4706](https://doi.org/10.22033/ESGF/CMIP6.4706).

748 EC-Earth-Consortium, 2020: EC-Earth-Consortium EC-Earth3-Veg-LR model output prepared
749 for CMIP6 CMIP historical. Earth System Grid Federation, [https://doi.org/10.22033/ESGF/](https://doi.org/10.22033/ESGF/CMIP6.4707)
750 [CMIP6.4707](https://doi.org/10.22033/ESGF/CMIP6.4707).

751 EC-Earth-Consortium, 2021: EC-Earth-Consortium EC-Earth-3-CC model output prepared for
752 CMIP6 CMIP historical. Earth System Grid Federation, [https://doi.org/10.22033/ESGF/CMIP6.](https://doi.org/10.22033/ESGF/CMIP6.4702)
753 [4702](https://doi.org/10.22033/ESGF/CMIP6.4702).

754 Eguíluz, V. M., J. Fernández-Gracia, X. Irigoien, and C. M. Duarte, 2016: A quantitative as-
755 sessment of Arctic shipping in 2010–2014. *Scientific Reports 2016 6:1*, **6**, 1–6, [https://doi.org/](https://doi.org/10.1038/srep30682)
756 [10.1038/srep30682](https://doi.org/10.1038/srep30682).

757 England, M., A. Jahn, and L. Polvani, 2019: Nonuniform contribution of internal vari-
758 ability to recent arctic sea ice loss. *Journal of Climate*, **32**, 4039–4053, [https://doi.org/](https://doi.org/10.1175/JCLI-D-18-0864.1)
759 [10.1175/JCLI-D-18-0864.1](https://doi.org/10.1175/JCLI-D-18-0864.1).

760 Fetterer, F., M. Savoie, S. Helfrich, and P. Clemente-Colón, 2010: Multisensor analyzed sea ice
761 extent - northern hemisphere (masie-nh), version 1. *U.S. National Ice Center and National Snow*
762 *and Ice Data Center*, <https://doi.org/10.7265/N5GT5K3K>.

763 Francis, J. A., and B. Wu, 2020: Why has no new record-minimum Arctic sea-ice extent occurred
764 since September 2012? *Environmental Research Letters*, **15**, [https://doi.org/10.1088/1748-9326/
765 abc047](https://doi.org/10.1088/1748-9326/abc047).

766 Giese, C., D. Notz, and J. Baehr, 2021: On the Origin of Discrepancies Between Observed
767 and Simulated Memory of Arctic Sea Ice. *Geophysical Research Letters*, **48**, [https://doi.org/
768 10.1029/2020GL091784](https://doi.org/10.1029/2020GL091784).

769 Goosse, H., O. Arzel, C. M. Bitz, A. D. Montety, and M. Vancoppenolle, 2009: Increased variability
770 of the Arctic summer ice extent in a warmer climate. *Geophysical Research Letters*, **36**, 1–5,
771 <https://doi.org/10.1029/2009GL040546>.

772 Gregory, W., J. Stroeve, and M. Tsamados, 2021: Network connectivity between the winter Arctic
773 Oscillation and summer sea ice in CMIP6 models and observations. *The Cryosphere*, 1653–1673.

774 Guemas, V., and Coauthors, 2016: A review on Arctic sea-ice predictability and prediction on
775 seasonal to decadal time-scales. *Quarterly Journal of the Royal Meteorological Society*, **142**,
776 546–561, <https://doi.org/10.1002/qj.2401>.

777 Hajima, T., and Coauthors, 2019: MIROC MIROC-ES2L model output prepared for CMIP6 CMIP
778 historical. Earth System Grid Federation, <https://doi.org/10.22033/ESGF/CMIP6.5602>.

779 Heo, E. S., M. K. Sung, S. I. An, and Y. M. Yang, 2021: Decadal phase shift of summertime Arctic
780 dipole pattern and its nonlinear effect on sea ice extent. *International Journal of Climatology*,
781 **41**, 4732–4742, <https://doi.org/10.1002/joc.7097>.

782 Hoerling, M. P., A. Kumar, and M. Zhong, 1997: El Niño, La Niña, and the Nonlinearity of Their
783 Teleconnections. *Journal of Climate*, **10** (8), 1769–1786, [https://doi.org/https://doi.org/10.1175/
784 1520-0442\(1997\)010<1769:ENOLNA>2.0.CO;2](https://doi.org/10.1175/1520-0442(1997)010<1769:ENOLNA>2.0.CO;2).

785 Holland, M. M., L. Landrum, D. Bailey, and S. Vavrus, 2019: Changing seasonal predictability
786 of Arctic summer sea ice area in a warming climate. *Journal of Climate*, **32**, 4963–4979,
787 <https://doi.org/10.1175/jcli-d-19-0034.1>.

788 Hu, C., S. Yang, Q. Wu, Z. Li, J. Chen, K. Deng, T. Zhang, and C. Zhang, 2016: Shifting El
789 Niño inhibits summer Arctic warming and Arctic sea-ice melting over the Canada Basin. *Nature
790 Communications*, **7**, 1–9, <https://doi.org/10.1038/ncomms11721>.

- 791 Huang, W., 2019: THU CIESM model output prepared for CMIP6 CMIP historical. Earth System
792 Grid Federation, <https://doi.org/10.22033/ESGF/CMIP6.8843>.
- 793 Jahn, A., 2018: Reduced probability of ice-free summers for 1.5 °c compared to 2 °c warming.
794 *Nature Climate Change*, **8**, 409–413, <https://doi.org/10.1038/s41558-018-0127-8>.
- 795 Jeong, H., H.-S. Park, M. F. Stuecker, and S.-W. Yeh, 2022a: Distinct impacts of major El
796 Niño events on Arctic temperatures due to differences in eastern tropical Pacific sea surface
797 temperatures. *Sci. Adv*, **8**, 8278.
- 798 Jeong, H., H. S. Park, M. F. Stuecker, and S. W. Yeh, 2022b: Record Low Arctic Sea Ice Extent
799 in 2012 Linked to Two-Year La Niña-Driven Sea Surface Temperature Pattern. *Geophysical*
800 *Research Letters*, **49**, <https://doi.org/10.1029/2022GL098385>.
- 801 Joseph, V. R., 2022: Optimal ratio for data splitting. *Statistical Analysis and Data Mining*, **15**,
802 531–538, <https://doi.org/10.1002/sam.11583>.
- 803 Kalnay, E., and Coauthors, 1996: The NCEP/NCAR 40-Year Reanalysis Project. *Bulletin of*
804 *the American Meteorological Society*, **77**, 437–471, [https://doi.org/10.1175/1520-0477\(1996\)](https://doi.org/10.1175/1520-0477(1996)077<0437:TNYRP>2.0.CO;2)
805 [077<0437:TNYRP>2.0.CO;2](https://doi.org/10.1175/1520-0477(1996)077<0437:TNYRP>2.0.CO;2).
- 806 Kay, J. E., M. M. Holland, and A. Jahn, 2011: Inter-annual to multi-decadal Arctic sea ice extent
807 trends in a warming world. *Geophysical Research Letters*, **38**, 2–7, [https://doi.org/10.1029/](https://doi.org/10.1029/2011GL048008)
808 [2011GL048008](https://doi.org/10.1029/2011GL048008).
- 809 Kay, J. E., and Coauthors, 2022: Less Surface Sea Ice Melt in the CESM2 Improves Arctic Sea Ice
810 Simulation With Minimal Non-Polar Climate Impacts. *Journal of Advances in Modeling Earth*
811 *Systems*, **14**, <https://doi.org/10.1029/2021MS002679>.
- 812 Kim, H., S. W. Yeh, S. I. An, and S. Y. Song, 2020: Changes in the role of Pacific decadal oscillation
813 on sea ice extent variability across the mid-1990s. *Scientific Reports*, **10**, [https://doi.org/10.1038/](https://doi.org/10.1038/s41598-020-74260-0)
814 [s41598-020-74260-0](https://doi.org/10.1038/s41598-020-74260-0).
- 815 Klavans, J. M., A. C. Clement, M. A. Cane, and L. N. Murphy, 2022: The Evolving Role of External
816 Forcing in North Atlantic SST Variability over the Last Millennium. *Journal of Climate*, **35**,
817 2741–2754, <https://doi.org/10.1175/JCLI-D-21-0338.1>.

818 Knutti, R., D. Masson, and A. Gettelman, 2013: Climate model genealogy: Generation CMIP5
819 and how we got there. *Geophysical Research Letters*, **40**, 1194–1199, <https://doi.org/10.1002/>
820 [grl.50256](https://doi.org/10.1002/grl.50256).

821 Kovacs, K. M., C. Lydersen, J. E. Overland, and S. E. Moore, 2011: Impacts of changing sea-
822 ice conditions on Arctic marine mammals. *Marine Biodiversity*, **41**, 181–194, <https://doi.org/>
823 [10.1007/s12526-010-0061-0](https://doi.org/10.1007/s12526-010-0061-0).

824 Krasting, J. P., and Coauthors, 2018: NOAA-GFDL GFDL-ESM4 model output prepared for
825 CMIP6 CMIP historical. Earth System Grid Federation, [https://doi.org/10.22033/ESGF/CMIP6.](https://doi.org/10.22033/ESGF/CMIP6.8597)
826 [8597](https://doi.org/10.22033/ESGF/CMIP6.8597).

827 Kwok, R., and D. A. Rothrock, 2009: Decline in Arctic sea ice thickness from submarine and
828 ICESat records: 1958-2008. *Geophysical Research Letters*, **36 (15)**, 1–5, [https://doi.org/10.](https://doi.org/10.1029/2009GL039035)
829 [1029/2009GL039035](https://doi.org/10.1029/2009GL039035).

830 Labe, Z. M., and E. A. Barnes, 2022: Comparison of climate model large ensembles with observa-
831 tions in the arctic using simple neural networks. *Earth and Space Science*, **9**, e2022EA002 348,
832 <https://doi.org/10.1029/2022EA002348>.

833 Lee, J., K. R. Sperber, P. J. Gleckler, K. E. Taylor, , Céline, and J. W. Bonfils, 2021: Benchmarking
834 Performance Changes in the Simulation of Extratropical Modes of Variability across CMIP
835 Generations. *Journal of Climate*, **34**, <https://doi.org/10.1175/JCLI-D-20>.

836 Lee, S., H. S. Park, S. Y. Song, and S. W. Yeh, 2023: Distinct impacts of two types of El
837 Niño events on northern winter high-latitude temperatures simulated by CMIP6 climate models.
838 *Environmental Research Letters*, **18**, <https://doi.org/10.1088/1748-9326/acbce9>.

839 Lenssen, N. J. L., G. A. Schmidt, J. E. Hansen, M. J. Menne, A. Persin, R. Ruedy, and D. Zyss,
840 2019: Improvements in the GISTEMP Uncertainty Model. *Journal of Geophysical Research:*
841 *Atmospheres*, **124**, 6307–6326, <https://doi.org/10.1029/2018JD029522>.

842 L'Heureux, M. L., A. Kumar, G. D. Bell, M. S. Halpert, and R. W. Higgins, 2008: Role of the
843 Pacific-North American (PNA) pattern in the 2007 Arctic sea ice decline. *Geophysical Research*
844 *Letters*, **35**, <https://doi.org/10.1029/2008GL035205>.

- 845 Li, D., R. Zhang, and T. Knutson, 2018a: Comparison of Mechanisms for Low-Frequency Vari-
846 ability of Summer Arctic Sea Ice in Three Coupled Models. *Journal of Climate*, **31**, 1205–1226,
847 <https://doi.org/10.1175/JCLI-D-16-0617.1>.
- 848 Li, F., Y. J. Orsolini, H. Wang, Y. Gao, and S. He, 2018b: Atlantic Multidecadal Oscillation
849 Modulates the Impacts of Arctic Sea Ice Decline. *Geophysical Research Letters*, **45**, 2497–2506,
850 <https://doi.org/10.1002/2017GL076210>.
- 851 Lindsay, R. W., and J. Zhang, 2006: Arctic ocean ice thickness: Modes of variability and the
852 best locations from which to monitor them. *Journal of Physical Oceanography*, **36**, 496–506,
853 <https://doi.org/10.1175/JPO2861.1>.
- 854 Liu, Z., and Coauthors, 2021: Acceleration of western Arctic sea ice loss linked to the Pacific North
855 American pattern. *Nature Communications*, **12**, <https://doi.org/10.1038/s41467-021-21830-z>.
- 856 Long, M., L. Zhang, S. Hu, and S. Qian, 2021: Multi-aspect assessment of CMIP6 models for Arctic
857 sea ice simulation. *Journal of Climate*, **34**, 1515–1529, [https://doi.org/10.1175/JCLI-D-20-0522.](https://doi.org/10.1175/JCLI-D-20-0522.1)
858 1.
- 859 Lovato, T., and D. Peano, 2020: CMCC CMCC-CM2-SR5 model output prepared for CMIP6
860 CMIP historical. Earth System Grid Federation, <https://doi.org/10.22033/ESGF/CMIP6.3825>.
- 861 McBride, L. A., A. P. Hope, T. P. Canty, B. F. Bennett, W. R. Tribett, and R. J. Salawitch,
862 2021: Comparison of CMIP6 historical climate simulations and future projected warming to
863 an empirical model of global climate. *Earth System Dynamics*, **12**, 545–579, [https://doi.org/](https://doi.org/10.5194/esd-12-545-2021)
864 [10.5194/esd-12-545-2021](https://doi.org/10.5194/esd-12-545-2021).
- 865 Meehl, G. A., C. T. Chung, J. M. Arblaster, M. M. Holland, and C. M. Bitz, 2018: Tropical
866 Decadal Variability and the Rate of Arctic Sea Ice Decrease. *Geophysical Research Letters*, **45**,
867 11,326–11,333, <https://doi.org/10.1029/2018GL079989>.
- 868 Melia, N., K. Haines, E. Hawkins, and J. J. Day, 2017: Towards seasonal Arctic shipping route
869 predictions. *Environmental Research Letters*, **12**, 084 005, [https://doi.org/10.1088/1748-9326/](https://doi.org/10.1088/1748-9326/AA7A60)
870 [AA7A60](https://doi.org/10.1088/1748-9326/AA7A60).

871 Miles, M. W., D. V. Divine, T. Furevik, E. Jansen, M. Moros, and A. E. Ogilvie, 2014: A signal of
872 persistent Atlantic multidecadal variability in Arctic sea ice. *Geophysical Research Letters*, **41**,
873 463–469, <https://doi.org/10.1002/2013GL058084>.

874 Milinski, S., N. Maher, and D. Olonscheck, 2020: How large does a large ensemble need to be?
875 *Earth Syst. Dynam.*, **11**, 885–901, <https://doi.org/10.5194/esd-11-885-2020>.

876 Mioduszewski, J. R., S. Vavrus, M. Wang, M. Holland, and L. Landrum, 2019: Past and future
877 interannual variability in Arctic sea ice in coupled climate models. *Cryosphere*, **13**, 113–124,
878 <https://doi.org/10.5194/tc-13-113-2019>.

879 Murphy, L. N., J. M. Klavans, A. C. Clement, and M. A. Cane, 2021: Investigating the Roles
880 of External Forcing and Ocean Circulation on the Atlantic Multidecadal SST Variability in a
881 Large Ensemble Climate Model Hierarchy. *Journal of Climate*, 1–51, <https://doi.org/10.1175/JCLI-D-20-0167.1>.

882

883 NASA Goddard Institute for Space Studies, 2018: NASA-GISS GISS-E2.1G model output prepared
884 for CMIP6 CMIP historical. Earth System Grid Federation, [https://doi.org/10.22033/ESGF/](https://doi.org/10.22033/ESGF/CMIP6.7127)
885 [CMIP6.7127](https://doi.org/10.22033/ESGF/CMIP6.7127).

886 NASA Goddard Institute for Space Studies, 2019a: NASA-GISS GISS-E2-2-G model output
887 prepared for CMIP6 CMIP historical. Earth System Grid Federation, [https://doi.org/10.22033/](https://doi.org/10.22033/ESGF/CMIP6.7129)
888 [ESGF/CMIP6.7129](https://doi.org/10.22033/ESGF/CMIP6.7129).

889 NASA Goddard Institute for Space Studies, 2019b: NASA-GISS GISS-E2.1H model output
890 prepared for CMIP6 CMIP historical. Earth System Grid Federation, [https://doi.org/10.22033/](https://doi.org/10.22033/ESGF/CMIP6.7128)
891 [ESGF/CMIP6.7128](https://doi.org/10.22033/ESGF/CMIP6.7128).

892 NASA Goddard Institute for Space Studies, 2019c: NASA-GISS GISS-E2.2H model out-
893 put prepared for CMIP6 CMIP historical. Earth System Grid Federation, [https://doi.org/](https://doi.org/10.22033/ESGF/CMIP6.15871)
894 [10.22033/ESGF/CMIP6.15871](https://doi.org/10.22033/ESGF/CMIP6.15871).

895 Neubauer, D., and Coauthors, 2019: HAMMOZ-Consortium MPI-ESM1.2-HAM model output
896 prepared for CMIP6 CMIP historical. Earth System Grid Federation, [https://doi.org/10.22033/](https://doi.org/10.22033/ESGF/CMIP6.5016)
897 [ESGF/CMIP6.5016](https://doi.org/10.22033/ESGF/CMIP6.5016).

- 898 Notz, D., 2015: How well must climate models agree with observations? *Philosophical*
899 *Transactions of the Royal Society A: Mathematical, Physical and Engineering Sciences*, **373**,
900 <https://doi.org/10.1098/rsta.2014.0164>.
- 901 Notz, D., and J. Stroeve, 2016: Observed Arctic sea-ice loss directly follows anthropogenic CO2
902 emission. *Science*, **354**, 747–750, <https://doi.org/10.1126/science.aag2345>.
- 903 Olonscheck, D., T. Mauritsen, and D. Notz, 2019: Arctic sea-ice variability is primarily driven
904 by atmospheric temperature fluctuations. *Nature Geoscience*, **12**, 430–434, <https://doi.org/10.1038/s41561-019-0363-1>.
- 906 Onarheim, I. H., T. Eldevik, L. H. Smedsrud, and J. C. Stroeve, 2018: Seasonal and regional
907 manifestation of Arctic sea ice loss. *Journal of Climate*, **31**, 4917–4932, [https://doi.org/10.1175/](https://doi.org/10.1175/JCLI-D-17-0427.1)
908 [JCLI-D-17-0427.1](https://doi.org/10.1175/JCLI-D-17-0427.1).
- 909 O’neill, B. C., and Coauthors, 2016: The Scenario Model Intercomparison Project (ScenarioMIP)
910 for CMIP6. *Geosci. Model Dev*, **9**, 3461–3482, <https://doi.org/10.5194/gmd-9-3461-2016>.
- 911 Petrick, S., K. Riemann-Campe, S. Hoog, C. Growitsch, H. Schwind, R. Gerdes, and K. Rehdanz,
912 2017: Climate change, future Arctic Sea ice, and the competitiveness of European Arctic
913 offshore oil and gas production on world markets. *Ambio*, **46**, 410–422, [https://doi.org/10.1007/](https://doi.org/10.1007/s13280-017-0957-z)
914 [s13280-017-0957-z](https://doi.org/10.1007/s13280-017-0957-z).
- 915 Phillips, A., C. Deser, and J. Fasullo, 2014: A New Tool for Evaluating Modes of Variability in
916 Climate Models. *Eos*, **95**, 453–455, <https://doi.org/10.1002/2014EO490002>.
- 917 Rayner, N. A., D. E. Parker, E. B. Horton, C. K. Folland, L. V. Alexander, D. P. Rowell, E. C. Kent,
918 and A. Kaplan, 2003: Global analyses of sea surface temperature, sea ice, and night marine air
919 temperature since the late nineteenth century. *Journal of Geophysical Research: Atmospheres*,
920 **108**, 4407, <https://doi.org/10.1029/2002jd002670>.
- 921 Ridley, J., M. Menary, T. Kuhlbrodt, M. Andrews, and T. Andrews, 2019a: MOHC HadGEM3-
922 GC31-LL model output prepared for CMIP6 CMIP historical. Earth System Grid Federation,
923 <https://doi.org/10.22033/ESGF/CMIP6.6109>.

924 Ridley, J., M. Menary, T. Kuhlbrodt, M. Andrews, and T. Andrews, 2019b: MOHC HadGEM3-
925 GC31-MM model output prepared for CMIP6 CMIP historical. Earth System Grid Federation,
926 <https://doi.org/10.22033/ESGF/CMIP6.6112>.

927 Rong, X., 2019: CAMS CAMS-CSM1.0 model output prepared for CMIP6 CMIP historical. Earth
928 System Grid Federation, <https://doi.org/10.22033/ESGF/CMIP6.9754>.

929 Schupfner, M., and Coauthors, 2019: DKRZ MPI-ESM1.2-HR model output prepared for CMIP6
930 historical. Earth System Grid Federation, <https://doi.org/10.22033/ESGF/CMIP6.6594>.

931 Screen, J. A., and C. Deser, 2019: Pacific Ocean Variability Influences the Time of Emergence of a
932 Seasonally Ice-Free Arctic Ocean. *Geophysical Research Letters*, **46**, 2222–2231, [https://doi.org/](https://doi.org/10.1029/2018GL081393)
933 [10.1029/2018GL081393](https://doi.org/10.1029/2018GL081393).

934 Seferian, R., 2018: CNRM-CERFACS CNRM-ESM2-1 model output prepared for CMIP6 CMIP
935 historical. Earth System Grid Federation, <https://doi.org/10.22033/ESGF/CMIP6.4068>.

936 Seland, y., and Coauthors, 2019: NCC NorESM2-LM model output prepared for CMIP6 CMIP
937 historical. Earth System Grid Federation, <https://doi.org/10.22033/ESGF/CMIP6.8036>.

938 Serreze, M. C., M. M. Holland, and J. Stroeve, 2007: Perspectives on the Arctic’s Shrinking
939 Sea-Ice Cover. *Science*, **315 (5818)**, 1533–1536, <https://doi.org/10.1126/science.1139426>.

940 Sigmond, M., J. C. Fyfe, and N. C. Swart, 2018: Ice-free Arctic projections under the Paris
941 Agreement. *Nature Climate Change*, **8**, 404–408, <https://doi.org/10.1038/s41558-018-0124-y>.

942 Simon, A., G. Gastineau, C. Frankignoul, V. Lapin, and P. Ortega, 2022: Pacific Decadal Oscillation
943 modulates the Arctic sea-ice loss influence on the midlatitude atmospheric circulation in winter.
944 *Weather and Climate Dynamics*, **3**, 845–861, <https://doi.org/10.5194/wcd-3-845-2022>.

945 Song, Z., F. Qiao, Y. Bao, Q. Shu, Y. Song, and X. Yang, 2019: FIO-QLNM FIO-ESM2.0 model
946 output prepared for CMIP6 CMIP historical. Earth System Grid Federation, [https://doi.org/](https://doi.org/10.22033/ESGF/CMIP6.9199)
947 [10.22033/ESGF/CMIP6.9199](https://doi.org/10.22033/ESGF/CMIP6.9199).

948 Stroeve, J., M. M. Holland, W. Meier, T. Scambos, and M. Serreze, 2007: Arctic sea
949 ice decline: Faster than forecast. *Geophysical Research Letters*, **34**, 9501, [https://doi.org/](https://doi.org/10.1029/2007GL029703)
950 [10.1029/2007GL029703](https://doi.org/10.1029/2007GL029703).

951 Swart, N. C., J. C. Fyfe, E. Hawkins, J. E. Kay, and A. Jahn, 2015: Influence of internal variability
952 on arctic sea-ice trends. *Nature Climate Change*, **5**, 86–89, <https://doi.org/10.1038/nclimate2483>.

953 Swart, N. C., and Coauthors, 2019a: CCCma CanESM5-CanOE model output prepared for CMIP6
954 CMIP historical. Earth System Grid Federation, <https://doi.org/10.22033/ESGF/CMIP6.10260>.

955 Swart, N. C., and Coauthors, 2019b: CCCma CanESM5 model output prepared for CMIP6 CMIP
956 historical. Earth System Grid Federation, <https://doi.org/10.22033/ESGF/CMIP6.3610>.

957 Tang, Y., S. Rumbold, R. Ellis, D. Kelley, J. Mulcahy, A. Sellar, J. Walton, and C. Jones, 2019:
958 MOHC UKESM1.0-LL model output prepared for CMIP6 CMIP historical. Earth System Grid
959 Federation, <https://doi.org/10.22033/ESGF/CMIP6.6113>.

960 Tatebe, H., and M. Watanabe, 2018: MIROC MIROC6 model output prepared for CMIP6 CMIP
961 historical. Earth System Grid Federation, <https://doi.org/10.22033/ESGF/CMIP6.5603>.

962 Tietsche, S., and Coauthors, 2014: Seasonal to interannual Arctic sea ice predictability in current
963 global climate models. *Geophysical Research Letters*, **41**, 1035–1043, [https://doi.org/10.1002/](https://doi.org/10.1002/2013GL058755)
964 [2013GL058755](https://doi.org/10.1002/2013GL058755).

965 Topál, D., Q. Ding, J. Mitchell, I. Baxter, M. Herein, T. Haszpra, R. Luo, and Q. Li, 2020: An
966 internal atmospheric process determining summertime Arctic sea ice melting in the next three
967 decades: Lessons learned from five large ensembles and multiple CMIP5 climate simulations.
968 *Journal of Climate*, **33**, 7431–7454, <https://doi.org/10.1175/JCLI-D-19-0803.1>.

969 Ukita, J., M. Honda, H. Nakamura, Y. Tachibana, D. J. Cavalieri, C. L. Parkinson, H. Koide,
970 and K. Yamamoto, 2007: Northern Hemisphere sea ice variability: Lag structure and its
971 implications. *Tellus, Series A: Dynamic Meteorology and Oceanography*, **59** (2), 261–272,
972 <https://doi.org/10.1111/j.1600-0870.2006.00223.x>.

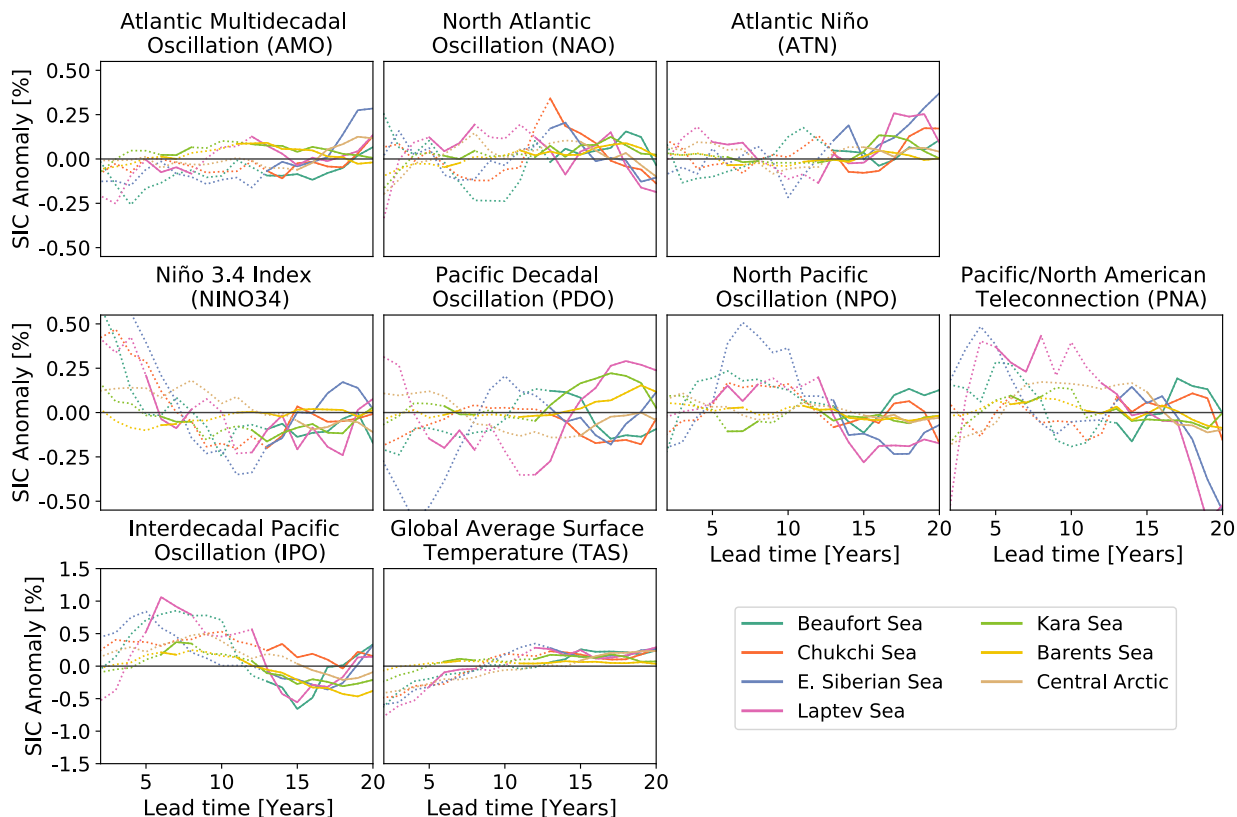
973 VanAchter, G., L. Ponsoni, F. Massonnet, T. Fichet, and V. Legat, 2020: Brief communication:
974 Arctic sea ice thickness internal variability and its changes under historical and anthropogenic
975 forcing. *Cryosphere*, **14**, 3479–3486, <https://doi.org/10.5194/tc-14-3479-2020>.

976 Voldoire, A., 2018: CNRM-CERFACS CNRM-CM6-1 model output prepared for CMIP6 CMIP
977 historical. Earth System Grid Federation, <https://doi.org/10.22033/ESGF/CMIP6.4066>.

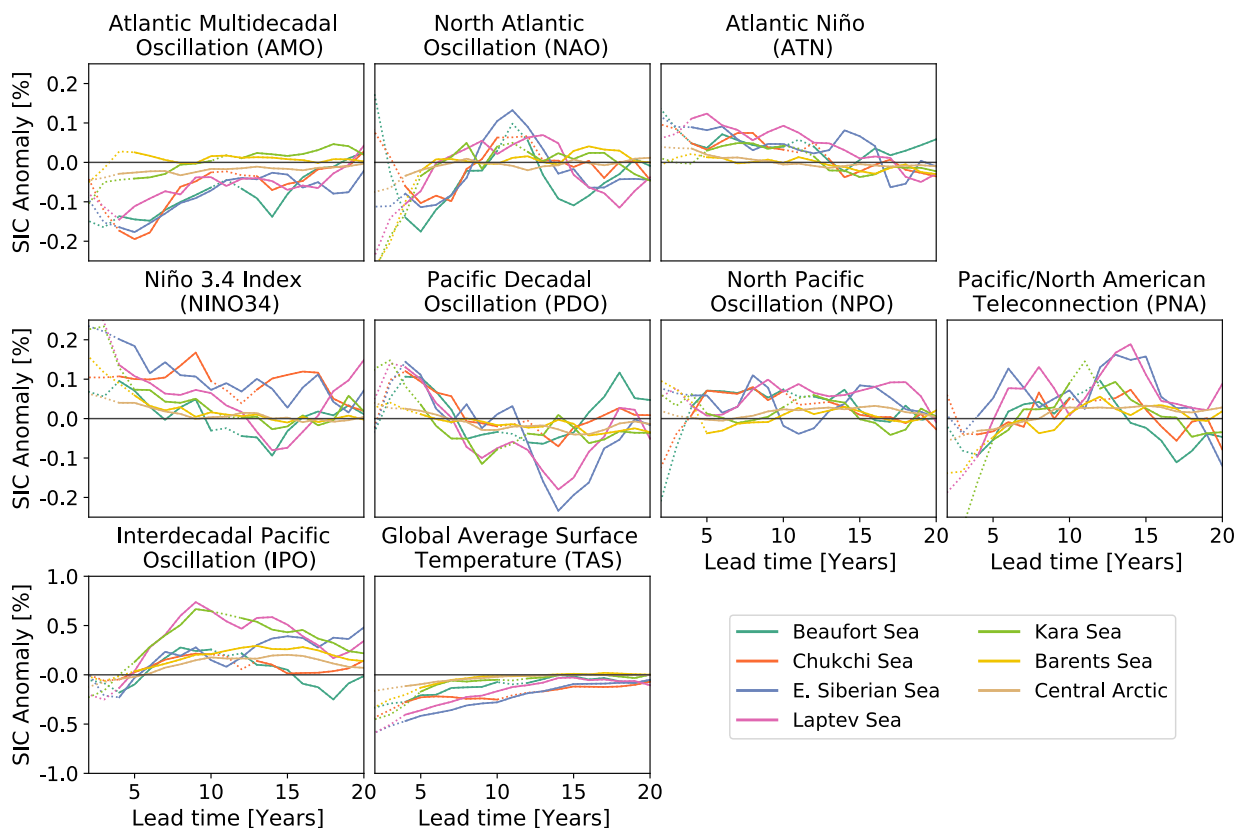
- 978 Volodin, E., and Coauthors, 2019: INM INM-CM5-0 model output prepared for CMIP6 CMIP
979 historical. Earth System Grid Federation, <https://doi.org/10.22033/ESGF/CMIP6.5070>.
- 980 Wang, M., and J. E. Overland, 2012: A sea ice free summer Arctic within 30 years:
981 An update from CMIP5 models. *Geophysical Research Letters*, **39**, 6–11, [https://doi.org/](https://doi.org/10.1029/2012GL052868)
982 [10.1029/2012GL052868](https://doi.org/10.1029/2012GL052868).
- 983 Wang, Q., S. Danilov, L. Mu, D. Sidorenko, and C. Wekerle, 2021: Lasting impact of winds
984 on Arctic sea ice through the ocean’s memory. *Cryosphere*, **15**, 4703–4725, [https://doi.org/](https://doi.org/10.5194/tc-15-4703-2021)
985 [10.5194/tc-15-4703-2021](https://doi.org/10.5194/tc-15-4703-2021).
- 986 Watanabe, S., and Coauthors, 2021: MIROC MIROC-ES2H model output prepared for CMIP6
987 CMIP historical. Earth System Grid Federation, <https://doi.org/10.22033/ESGF/CMIP6.5601>.
- 988 Weijer, W., W. Cheng, O. A. Garuba, A. Hu, and B. T. Nadiga, 2020: CMIP6 Models Predict Sig-
989 nificant 21st Century Decline of the Atlantic Meridional Overturning Circulation. *Geophysical*
990 *Research Letters*, **47**, <https://doi.org/10.1029/2019GL086075>.
- 991 Wieners, K.-H., and Coauthors, 2019: MPI-M MPIESM1.2-LR model output prepared for CMIP6
992 historical. Earth System Grid Federation, <https://doi.org/10.22033/ESGF/CMIP6.6595>.
- 993 Wu, T., and Coauthors, 2018: BCC BCC-CSM2MR model output prepared for CMIP6 CMIP
994 historical. Earth System Grid Federation, <https://doi.org/10.22033/ESGF/CMIP6.2948>.
- 995 Wyburn-Powell, C., A. Jahn, and M. England, 2022: Modeled Interannual Variability of Arctic
996 Sea Ice Cover is Within Observational Uncertainty. *Journal of Climate*, 1–35, [https://doi.org/](https://doi.org/10.1175/jcli-d-21-0958.1)
997 [10.1175/jcli-d-21-0958.1](https://doi.org/10.1175/jcli-d-21-0958.1).
- 998 Yeager, S. G., A. R. Karspeck, and G. Danabasoglu, 2015: Predicted slowdown in the rate of
999 Atlantic sea ice loss. *Geophysical Research Letters*, **42**, 10 704–10 713, [https://doi.org/10.1002/](https://doi.org/10.1002/2015GL065364)
1000 [2015GL065364](https://doi.org/10.1002/2015GL065364).
- 1001 Yukimoto, S., and Coauthors, 2019: MRI MRI-ESM2.0 model output prepared for CMIP6 CMIP
1002 historical. Earth System Grid Federation, <https://doi.org/10.22033/ESGF/CMIP6.6842>.
- 1003 Zhang, J., and Coauthors, 2018: BCC BCC-ESM1 model output prepared for CMIP6 CMIP
1004 historical. Earth System Grid Federation, <https://doi.org/10.22033/ESGF/CMIP6.2949>.

- 1005 Zhang, M., W. Perrie, and Z. Long, 2019: Springtime North Pacific Oscillation and summer
1006 sea ice in the Beaufort sea. *Climate Dynamics*, **53 (1-2)**, 671–686, [https://doi.org/10.1007/](https://doi.org/10.1007/s00382-019-04627-1)
1007 [s00382-019-04627-1](https://doi.org/10.1007/s00382-019-04627-1).
- 1008 Zhang, R., and J. M. Wallace, 2015: Mechanisms for low-frequency variability of summer Arctic
1009 sea ice extent. *Proceedings of the National Academy of Sciences of the United States of America*,
1010 **112**, <https://doi.org/10.1073/pnas.1422296112>.
- 1011 Zhang, S., T. Y. Gan, and A. B. Bush, 2020: Variability of Arctic sea ice based on quantile
1012 regression and the teleconnection with large-scale climate patterns. *Journal of Climate*, **33 (10)**,
1013 4009–4025, <https://doi.org/10.1175/JCLI-D-19-0375.1>.
- 1014 Ziehn, T., and Coauthors, 2019: CSIRO ACCESS-ESM1.5 model output prepared for CMIP6
1015 CMIP historical. Earth System Grid Federation, <https://doi.org/10.22033/ESGF/CMIP6.4272>.
- 1016 Årthun, M., I. H. Onarheim, J. Dörr, and T. Eldevik, 2021: The Seasonal and Regional Transition
1017 to an Ice-Free Arctic. *Geophysical Research Letters*, **48**, e2020GL090825, [https://doi.org/10.](https://doi.org/10.1029/2020GL090825)
1018 [1029/2020GL090825](https://doi.org/10.1029/2020GL090825).

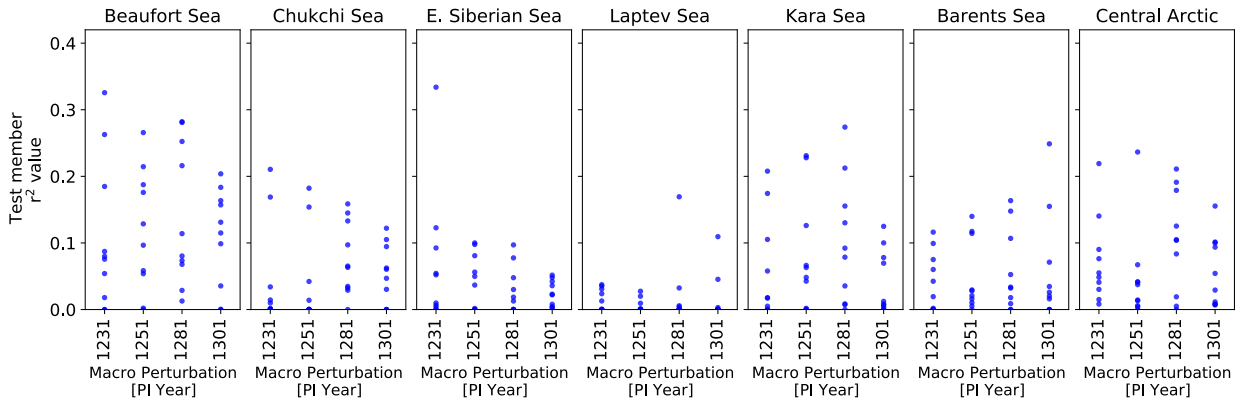
Supplementary Material



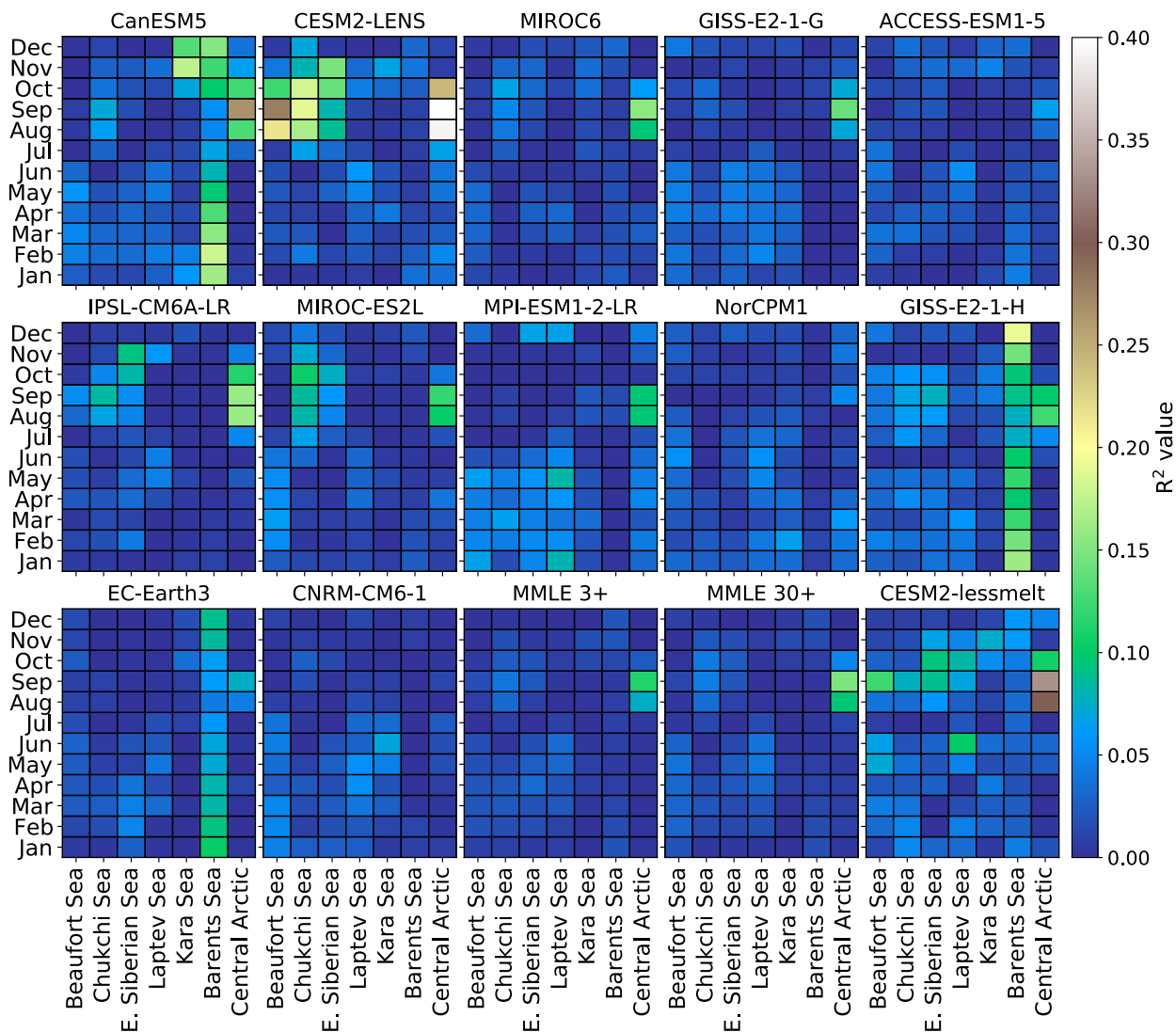
1019 **FIG. S1. Linear drivers of regional sea ice concentration anomalies for a reduced time period.** Same as
 1020 Figure 4, except for the reduced time period of 1970-2014 instead of 1920-2014. By comparing this figure with
 1021 4, we can see that the modes of variability have a similar influence as for the 1920-2014 time period, although
 1022 the results are far more noisy and predictive skill does not exceed persistence for as much of the lead times as for
 1023 the period 1920-2014.



1024 **FIG. S2. Linear drivers of regional sea ice concentration anomalies for pre-industrial control runs.**
 1025 Same as Figure 4 and S1, except here using the 1850 control simulations instead of the period 1920-2014 in the
 1026 historical simulations. As for Fig. S1, the influence of the climate variability modes are very similar as for the
 1027 period 1920-2014 (Fig. 4), but the coefficients are smaller, likely due to the lower variability in the pre-industrial
 1028 mean state. Instead of different ensemble members, the available 35 GCMs are each split into several members
 1029 of 74 year length each, with the first 222 years used for training and the following 74 years for validation.



1030 **FIG. S3. Influence of macro versus micro initializations in the CESM2-LENS on September test member**
 1031 **r^2 values.** Of the 48 test members from the CESM2-LENS, 12 are created through macro initializations by
 1032 choosing different start years from the pre-industrial simulation, and hence differ in their ocean and atmospheric
 1033 state. Of those 12, four (here shown on the x-axis by branch year) have 9 additional ensemble members branched
 1034 from them, which all only differ slightly in their atmospheric state due to small atmospheric perturbations,
 1035 i.e., referred to as micro initializations. Here we show these latter 40 simulations (blue circles), to assess
 1036 whether macro or micro initializations dominate the possible r^2 values (with persistence removed). As the four
 1037 distributions of 10 realizations for each macro initialization are very similar, this shows that the ocean state
 1038 (macro perturbation) has a much smaller impact on prediction skill than atmospheric micro perturbations.



1039 FIG. S4. Persistence r^2 values for LEs, MMLEs, and CESM2-lessmelt at a 5-year lag time. This figure
 1040 shows the persistence r^2 value that was subtracted from the absolute value of the validation r^2 in Figure 3.
 1041 Additionally the CESM2-lessmelt persistence is shown for comparison with CESM2-LENS. CESM2-lessmelt
 1042 has a thicker sea ice mean state than CESM2-LEMS and, as shown in this figure, has a smaller persistence
 1043 validation r^2 value, although this value is still an outlier compared with the other GCMs.